Table 3
Genes whose expression was down-regulated by $KBrO_3$ (2.5 mM, 4 h)

	Gene symbol	Ratio	Gene title
Cell cycle, cell growth	FH	0.51	Fumarate hydratase
	MYC	0.55	v-myc myelocytomatosis viral oncogene homolog
Signal transduction	DUSP2	0.37	Dual specificityphosphatase 2
	RRBP1	0.39	Ribosome binding protein 1 homolog 180 kDa
	TBL3	0 43	Transducin (beta)-like3
Transcription regulation	CITED2	0.45	Cbp/p300-interacting transactivator, with Glu/Asp-rich carboxy-terminal domain, 2
	KIAA1196	0.43	KIAA1196 protein
	TZFP	0 39	Testis zinc finger protein
Chromosome organization	H1FX	0.14	H1 histone family member X
Protein modification	CLTB	0.43	Clathrin, light polypeptide (Lcb)
Energy pathway	FDX1	0.45	Ferredoxin 1
	QPRT	0.41	Quinolinate phosphoribosyltransferase
	SLC39A4	0.43	Solute carrier family 39 (zinc transporter), member 4
Unclassified	BTBD2	0.35	BTB (POZ) domain containing 2
	LOC339229	0.44	Hypothetical protein LOC339229
	MGRN1	0.44	Mahogunin, ring finger 1
	MRP63	0.41	Mitochondrial ribosomal protein 63
	PHLDA1	0.43	Pleckstrin homology-like domain, family A, member 1
	PTPLA	0.37	Protein tyrosine phosphatase-like (proline instead of catalytic arginine), member a
	SPATA2	0.45	Spermatogenesis associated 2

examined the mutagenicity of a hydroxyl radical generator, *N,N'*-bis (2-hydroxyperoxy-2-methoxyethyl)-1,4,5,8-naphthalene-tetra-carboxylic diimide (NP-III). Although NP-III highly produced 8OHdG upon irradiation with UV in V79 cells, the frequency of *Hprt* gene mutation was not significantly induced [34]. Molecular analysis demonstrated the no association of induction of 8OHdG with GC > TA transversion in the *Hprt* mutants [35]. 8OHdG is mainly removed by Ogg1 protein in a manor of the base excision repair (BER) pathway. Arai et al. investigated the relationship between the accumulation of oxidative DNA damage and the induction of gene mutation using *Ogg*1 deficient transgenic mice [36]. Although the 8OHdG level in kidneys of the *Ogg*1 deficient mice increase 200 times of the control level after 4 weeks' $KBrO_3$ treatment, the mutation frequency in the transgenic *gpt* gene was induced by less than 10 times of the control level. The molecular analysis revealed that the fraction of GC > TA transversions did not specifically increased. These results suggest that 8OHdG-mediated base substitutions do not mainly contribute to the mutagenic process involved in $KBrO_3$-induced carcinogenesis. Other genotoxic events must be involved in the carcinogenic process.

Our present studies strongly support this hypothesis. We demonstrated that $KBrO_3$ treatment clearly induced DNA damage in both the alkaline and neutral COM assay (Fig. 1). The alkaline COM assay is capable of detecting any DNA damages including DSB, single strand breaks (SSB), alkali-labile sites, DNA–DNA/DNA–protein cross-linking, and SSB associated with incomplete excision repair sites, while the neutral COM assay allows the detection of DSB, considered to be "biologically relevant" lesion of radiation damage [24]. $KBrO_3$ may have radio-mimic genotoxicity that yields oxidative DNA damage as well as DSB. $KBrO_3$ also induced MN formation and *TK* gene mutation significantly in TK6 cells. In the *TK* gene mutation assay, $KBrO_3$ predominantly produced SG mutants, but not NG mutants (Fig. 1c), implying that gross structural changes such as deletion and recombination are associated with the mutations. Molecular analysis of the *TK* mutants confirmed the assumption. Most of *TK* mutants showed LOH mutations, not non-LOH mutations, which are mainly point mutations. Harrington-Brock et al. also demonstrated that bromate compounds significantly induced *Tk* mutations in mouse lymphoma L5178Y cells, and almost all were LOH mutations [5]. LOH can be caused by deletions,

mitotic recombination between homologous alleles, or whole chromosome loss [20]. Molecular analysis can distinguish between them and reveal the mechanism and the characteristics of the mutants. In this study, $KBrO_3$ predominantly induced large deletions that resulted in hemizygous LOH (Table 1). The large deletions were mainly terminal deletions in the proximal region of chromosome 17q, which were rarely observed in spontaneously arising *TK* mutants (Fig. 3). The mutational spectrum and LOH pattern induced by $KBrO_3$ were similar to those induced by X-irradiation (Figs. 2 and 3) [20,21]. DSBs induced X-rays cause large deletions [19,20]. When the DSBs are repaired by the non-homologous end-joining pathway, interstitial deletions result. The broken chromosome ends can be also stabilized by the addition of new telomere sequences. Because TK6 cells have high telomerase activity [20], the result is terminal deletions. Thus, the major genotoxicity of $KBrO_3$ may be due to DSBs, but not to 8OHdG converting GC > TA transversion.

Some 8OHdG lesions can convert DSBs through the BER pathway [37]. In the initial step of BER, Ogg1 removes 8OHdG by DNA glycosylase activity and nicks the DNA backbone because of its associated lyase activity. The resulting SSB is processed by an apurinic endonuclease, which generates a single nucleotide gap. The gap is filled in by a DNA polymerase and sealed by a DNA ligase [38]. Clustered 8OHdG lesions induced by $KBrO_3$ may not be appropriately repaired by BER and cause DSB, however, because it is possible that two closely opposed 8OHdGs convert two closely opposed SSBs by BER resulting DSB [39,40]. Yang et al. developed Ogg1 over-expressing TK6 cell (TK6-hOGG1) and examined cytotoxic and mutagenic responses to gamma-irradiation [41]. They demonstrated that TK6-hOGG1 cells are more sensitive than the parental TK6 cells to cytotoxicity and mutagenicity by gamma-irradiation, and most of the induced *TK* mutants in TK6-OGG1 exhibited SG phenotype, which were probably large deletion mutants resulted by DSBs. This result clearly indicates that BER pathway contributes to convert oxidative damages to DSBs. Some clustered 8OHdG induced by $KBrO_3$ may covert to DSBs in TK6 cells, because TK6 is Ogg1 proficient cells [37].

To clarify the genotoxic characteristics of $KBrO_3$, we investigated the gene expression profile using Affymetrix GeneChip® Expression analysis. Many genes were up- or down-regulated by exposure to 2.5 mM $KBrO_3$ (Tables 2 and 3). Akerman et al. investigated the alterations of gene expression profiles in ionizing radiation-exposed TK6 cells [42]. They reported a >50% increase in expression of ATF-3 (stress response), Cyclin G (cell cycle), FAS antigen (apoptosis), GADD45 (repair and apoptosis), PCNA (repair), Rad51 (repair), and p21 (cell cycle) and a 40% decrease in expression of c-Myc (transcription factor), interferon stimulatory gene factor-3 (cell signaling), and p55CDC (cell cycle). We also observed up-regulation of p21 and down-regulation of c-Myc. Up-regulation of p21, however, is observed in TK6 cells exposed to any DNA-damaging chemical [43]. Islaih et al. also demonstrated the relationship between the gene expression profiles and the DNA damaging agents using TK6 cells [43]. They examined six chemicals including H_2O_2 and bleomycin which induce oxidative DNA damage. Although 10 genes were commonly up-regulated between H_2O_2 and bleomycin treatments, these genes except for p21 were not observed in our experiment. Thus, we could not find the similarity of gene expression profile by the treatment with $KBrO_3$ to by the treatment with ionizing radiation as well as oxidative damage inducers. Comparing gene expression profiles across platforms, laboratories, and experiments must be difficult [44]. Although it is difficult to judge from the expression analysis of the single chemical, information on genes which altered their expression gives a clue to understand the mechanism of action. Firstly, predominance of DNA repair and cell cycle related genes in up-regulated genes supports the genotoxic action of $KBrO_3$. Up-regulation of stress genes and apoptosis related genes suggests an involvement of oxidative stress. Up-regulation of catalase may be responsible for the oxidative damage by $KBrO_3$ (Table 2). Unclassified genes for alteration may have a functional relationship with genotoxic mechanism.

In conclusion, $KBrO_3$ predominantly induced large deletions at chromosomal level in human TK6 cells. The major genotoxicity leading to carcinogenesis of $KBrO_3$ may be due to DSBs rather than to 8OHdG adducts that lead to GC > TA transversions, as is commonly believed.

Acknowledgments

The TK6 cell line used in this study was a kind gift of Dr. John B. Little of the Harvard School of Public Health, Boston, MA. This study was supported by Health, Welfare, and Labor Science Research Grants (H15-chem-002, H15-food-004) in Japan.

References

[1] Y. Kurokawa, A. Maekawa, M. Takahashi, Y. Hayashi, Toxicity and carcinogenicity of potassium bromate—a new renal carcinogen, Environ. Health Perspect. 87 (1990) 309–335.

[2] Y. Kurokawa, S. Aoki, Y. Matsushima, N. Takamura, T. Imazawa, Y. Hayashi, Dose–response studies on the carcinogenicity of potassium bromate in F344 rats after long-term oral administration, J. Natl. Cancer Inst. 77 (1986) 977–982.
[3] A.B. DeAngelo, M.H. George, S.R. Kilburn, T.M. Moore, D.C. Wolf, Carcinogenicity of potassium bromate administered in the drinking water to male B6C3F1 mice and F344/N rats, Toxicol. Pathol. 26 (1998) 587–594.
[4] M. Ishidate Jr., K. Yoshikawa, Chromosome aberration tests with Chinese hamster cells in vitro with and without metabolic activation—a comparative study on mutagens and carcinogens, Arch. Toxicol. Suppl. 4 (1980) 41–44.
[5] K. Harrington-Brock, D.D. Collard, T. Chen, Bromate induces loss of heterozygosity in the thymidine kinase gene of L5178Y/Tk(±)-3.7.2C mouse lymphoma cells, Mutat. Res. 537 (2003) 21–28.
[6] M. Hayashi, T. Sofuni, M. Ishidate Jr., High-sensitivity in micronucleus induction of a mouse strain (MS), Mutat. Res. 105 (1982) 253–256.
[7] M. Hayashi, M. Kishi, T. Sofuni, M. Ishidate Jr., Micronucleus tests in mice on 39 food additives and eight miscellaneous chemicals, Food Chem. Toxicol. 26 (1988) 487–500.
[8] H. Kamiya, K. Miura, H. Ishikawa, H. Inoue, S. Nishimura, E. Ohtsuka, c-Ha-ras containing 8-hydroxyguanine at codon 12 induces point mutations at the modified and adjacent positions, Cancer Res. 52 (1992) 3483–3485.
[9] A.G. Knudson, Antioncogenes and human cancer, Proc. Natl. Acad. Sci. U.S.A. 90 (1993) 10914–10921.
[10] H. Kasai, S. Nishimura, Y. Kurokawa, Y. Hayashi, Oral administration of the renal carcinogen, potassium bromate, specifically produces 8-hydroxydeoxyguanosine in rat target organ DNA, Carcinogenesis 8 (1987) 1959–1961.
[11] K.C. Cheng, D.S. Cahill, H. Kasai, S. Nishimura, L.A. Loeb, 8-Hydroxyguanine, an abundant form of oxidative DNA damage, causes G–T and A–C substitutions, J. Biol. Chem. 267 (1992) 166–172.
[12] S. Shibutani, M. Takeshita, A.P. Grollman, Insertion of specific bases during DNA synthesis past the oxidation-damaged base 8-oxodG, Nature 349 (1991) 431–434.
[13] K. Sai, C.A. Tyson, D.W. Thomas, J.E. Dabbs, R. Hasegawa, Y. Kurokawa, Oxidative DNA damage induced by potassium bromate in isolated rat renal proximal tubules and renal nuclei, Cancer Lett. 87 (1994) 1–7.
[14] G. Speit, S. Haupter, P. Schutz, P. Kreis, Comparative evaluation of the genotoxic properties of potassium bromate and potassium superoxide in V79 Chinese hamster cells, Mutat. Res. 439 (1999) 213–221.
[15] T. Umemura, K. Sai, A. Takagi, R. Hasegawa, Y. Kurokawa, A possible role for oxidative stress in potassium bromate (KBrO3) carcinogenesis, Carcinogenesis 16 (1995) 593–597.
[16] K. Fujie, H. Shimazu, M. Matsuda, T. Sugiyama, Acute cytogenetic effects of potassium bromate on rat bone marrow cells in vivo, Mutat. Res. 206 (1988) 455–458.
[17] M. Ishidate Jr., T. Sofuni, K. Yoshikawa, M. Hayashi, T. Nohmi, M. Sawada, A. Matsuoka, Primary mutagenicity screening of food additives currently used in Japan, Food Chem. Toxicol. 22 (1984) 623–636.
[18] H.L. Liber, W.G. Thilly, Mutation assay at the thymidine kinase locus in diploid human lymphoblasts, Mutat. Res. 94 (1982) 467–485.
[19] H.L. Liber, D.W. Yandell, J.B. Little, A comparison of mutation induction at the tk and hprt loci in human lymphoblastoid cells; quantitative differences are due to an additional class of mutations at the autosomal tk locus, Mutat. Res. 216 (1989) 9–17.
[20] M. Honma, Generation of loss of heterozygosity and its dependency on p53 status in human lymphoblastoid cells, Environ. Mol. Mutagen. 45 (2005) 162–176.
[21] M. Honma, M. Hayashi, T. Sofuni, Cytotoxic and mutagenic responses to X-rays and chemical mutagens in normal and p53-mutated human lymphoblastoid cells, Mutat. Res. 374 (1997) 89–98.
[22] L. Zhan, H. Sakamoto, M. Sakuraba, D.S. Wu, L.S. Zhang, T. Suzuki, M. Hayashi, M. Honma, Genotoxicity of microcystin-LR in human lymphoblastoid TK6 cells, Mutat. Res. 557 (2004) 1–6.
[23] N. Koyama, H. Sakamoto, M. Sakuraba, T. Koizumi, Y. Takashima, M. Hayashi, H. Matsufuji, K. Yamagata, S. Masuda, N. Kinae, M. Honma, Genotoxicity of acrylamide and glycidamide in human lymphoblastoid TK6 cells, Mutat. Res. 603 (2006) 151–158.
[24] S. Wada, H. Kurahayashi, Y. Kobayashi, T. Funayama, K. Yamamoto, M. Natsuhori, N. Ito, The relationship between cellular radiosensitivity and radiation-induced DNA damage measured by the comet assay, J. Vet. Med. Sci. 65 (2003) 471–477.
[25] M. Watanabe-Akanuma, T. Ohta, Y.F. Sasaki, A novel aspect of thiabendasole as a photomutagen in bacteria and cultured human cells, Mutat. Res. 158 (2005) 213–219.
[26] T. Matsushima, M. Hayashi, A. Matsuoka, M. Ishidate Jr., K.F. Miura, H. Shimizu, Y. Suzuki, K. Morimoto, H. Ogura, K. Mure, K. Koshi, T. Sofuni, Validation study of the in vitro micronuclei test in a Chinese hamster lung cell line (CHL/IU), Mutagenesis 14 (1999) 569–580.
[27] T. Omori, M. Honma, M. Hayashi, Y. Honda, I. Yoshimura, A new statistical method for evaluating of L5178Ytk± mammalian cell data using microwell method 517 (2002) 199–208.
[28] M. Honma, M. Momose, H. Tanabe, H. Sakamoto, Y. Yu, J.B. Little, T. Sofuni, M. Hayashi, Requirement of wild-type p53 protein for maintenance of chromosomal integrity, Mol. Carcinog. 28 (2000) 203–214.
[29] P.L. Olive, DNA damage and repair in individual cells: applications of the comet assay in radiobiology, Int. J. Radiat. Biol. 75 (1999) 395–405.
[30] D.E. Levin, M. Hollstein, M.F. Christman, E.A. Schwiers, B.N. Ames, A new Salmonella tester strain (TA102) with A X T base pairs at the site of mutation detects oxidative mutagens, Proc. Natl. Acad. Sci. U.S.A. 79 (1982) 7445–7449.
[31] T. Arai, V.P. Kelly, O. Minowa, T. Noda, S. Nishimura, High accumulation of oxidative DNA damage, 8-hydroxyguanine, in Mmh/Ogg1 deficient mice by chronic oxidative stress, Carcinogenesis 23 (2002) 2005–2010.
[32] F. Le Page, A. Margot, A.P. Grollman, A. Sarasin, A. Gentil, Mutagenicity of a unique 8-oxoguanine in a human Ha-ras sequence in mammalian cells, Carcinogenesis 16 (1995) 2779–2784.
[33] M.L. Wood, M. Dizdaroglu, E. Gajewski, J.M. Essigmann, Mechanistic studies of ionizing radiation and oxidative mutagenesis: genetic effects of a single 8-hydroxyguanine (7-hydro-8-oxoguanine) residue inserted at a unique site in a viral genome, Biochemistry 29 (1990) 7024–7032.
[34] T. Takeuchi, S. Matsugo, K. Morimoto, Mutagenicity of oxidative DNA damage in Chinese hamster V79 cells, Carcinogenesis 18 (1997) 2051–2055.
[35] M. Nakajima, T. Takeuchi, K. Ogino, K. Morimoto, Lack of direct involvement of 8-hydroxy-2′-deoxyguanosine in

hypoxanthine-guanine phosphoribosyltransferase mutagenesis in V79 cells treated with *N,N'*-bis(2-hydroxyperoxy-2-methoxy-ethyl)-1,4,5,8-naphthalenetetracarboxyli c-diimide (NP-III) or riboflavin, Jpn. J. Cancer Res. 93 (2002) 247–252.

[36] T. Arai, V.P. Kelly, K. Komoro, O. Minowa, T. Noda, S. Nishimura, Cell proliferation in liver of Mmh/Ogg1-deficient mice enhances mutation frequency because of the presence of 8-hydroxyguanine in DNA, Cancer Res. 63 (2003) 4287–4292.

[37] N. Yang, M.A. Chaudhry, S.S. Wallace, Base excision repair by hNTH1 and hOGG1: a two edged sword in the processing of DNA damage in gamma-irradiated human cells, DNA Repair (Amst.) 5 (2006) 43–51.

[38] G. Slupphaug, B. Kavli, H.E. Krokan, The interacting pathways for prevention and repair of oxidative DNA damage, Mutat. Res. 531 (2003) 231–251.

[39] K. Tian, M. McTigue, S.C. de los, Sorting the consequences of ionizing radiation: processing of 8-oxoguanine/abasic site lesions, DNA Repair (Amst.) 1 (2002) 1039–1049.

[40] M.E. Lomax, S. Cunniffe, P. O'Neill, Efficiency of repair of an abasic site within DNA clustered damage sites by mammalian cell nuclear extracts, Biochemistry 43 (2004) 11017–11026.

[41] N. Yang, H. Galick, S.S. Wallace, Attempted base excision repair of ionizing radiation damage in human lymphoblastoid cells produces lethal and mutagenic double strand breaks, DNA Repair (Amst.) 3 (2004) 1323–1334.

[42] G.S. Akerman, B.A. Rosenzweig, O.E. Domon, C.A. Tsai, M.E. Bishop, L.J. McGarrity, J.T. Macgregor, F.D. Sistare, J.J. Chen, S.M. Morris, Alterations in gene expression profiles and the DNA-damage response in ionizing radiation-exposed TK6 cells, Environ. Mol. Mutagen. 45 (2005) 188–205.

[43] M. Islaih, B.W. Halstead, I.A. Kadura, B. Li, J.L. Reid-Hubbard, L. Flick, J.L. Altizer, D.J. Thom, D.K. Monteith, R.K. Newton, D.E. Watson, Relationships between genomic, cell cycle, and mutagenic responses of TK6 cells exposed to DNA damaging chemicals, Mutat. Res. 578 (2005) 100–116.

[44] C.L. Yauk, M.L. Berndt, A. Williams, G.R. Douglas, Comprehensive comparison of six microarray technologies, Nucleic Acids Res. 32 (2004) e124.

ELSEVIER

Experimental Hematology

Experimental Hematology 35 (2007) 1190–1200

Glycolytic inhibition by mutation of pyruvate kinase gene increases oxidative stress and causes apoptosis of a pyruvate kinase deficient cell line

Ken-ichi Aisaki[a], Shin Aizawa[b], Hisaichi Fujii[c], Jun Kanno[a], and Hitoshi Kanno[c,d,e]

[a]*Cellular and Molecular Toxicology Division, National Institute of Health and Sciences, Tokyo, Japan;* [b]*Department of Anatomy, Nihon University School of Medicine, Tokyo, Japan;* [c]*Department of Transfusion Medicine and Cell Processing;* [d]*Institute of Medical Genetics; and* [e]*Division of Genomic Medicine, Department of Advanced Biomedical Engineering and Science, Graduate School of Medicine, Tokyo Women's Medical University, Tokyo, Japan*

(Received 13 November 2006; revised 8 May 2007; accepted 9 May 2007)

Objective. **SLC3 is a Friend erythroleukemic cell line established from the *Pk-1*^{tlc} mouse, a mouse model of red blood cell type-pyruvate kinase (R-PK) deficiency. This study was aimed to elucidate the mechanisms attributing to apoptosis induced by R-PK deficiency.**

Materials and Methods. **SLC3 and a control Friend cell line, CBA2, were cultured in a condition of glucose deprivation or supplementation with 2-deoxyglucose, and apoptosis was detected by annexin V. We established two stable transfectants of SLC3 cells with human R-PK cDNA, and examined the effect of R-PK on an apoptotic feature by cell cycle analysis. Intracellular oxidation was measured with 2′,7′-dichlorofluorescin diacetate. DNA microarray analysis was performed to examine gene-expression profiles between the two transfectants and parental SLC3.**

Results. **SLC3 was more susceptible than CBA2 to apoptosis induced by glycolytic inhibition. The forced expression of R-PK significantly decreased cells at the sub G_0/G_1 stage in an expression-level dependent manner. Microarray analysis showed that proapoptotic genes, such as *Bad*, *Bnip3*, and *Bnip3l*, were downregulated in the transfectants. In addition, peroxiredoxin 1 (*Prdx1*) and other antioxidant genes, such as *Cat*, *Txnrd1*, and *Glrx1* were also downregulated. A significant decrease of dichlorofluorescein fluorescence was observed by R-PK expression. Preincubation with a glutathione precursor showed a significant decrease of apoptosis.**

Conclusion. **These results indicated that glycolytic inhibition by R-PK gene mutation augmented oxidative stress in the Friend erythroleukemia cell, leading to activation of hypoxia-inducible factor-1 as well as downstream proapoptotic gene expression. Thus, R-PK plays an important role as an antioxidant during erythroid differentiation.** © **2007 ISEH - Society for Hematology and Stem Cells. Published by Elsevier Inc.**

Glycolysis is an essential metabolic pathway in all organisms. Pyruvate kinase (PK) is a key glycolytic enzyme, and has four isoenzymes in mammals, designated M_1, M_2, L (liver), and R (red blood cell). In humans, these isozymes are encoded by two structural genes, *PKM* and *PKLR*, respectively [1]. M_2-PK is the only isozyme that is active in early fetal tissues and also almost ubiquitously expressed in adult tissues, including hematopoietic stem cells, progenitors, leukocytes, and platelets. Red blood cell type-pyruvate kinase (R-PK) becomes a major isozyme during erythroid differentiation/maturation [2,3], and in mature red blood cells (RBCs), R-PK is the only detectable PK isozyme. Deficiency of R-PK causes shortened RBC survival, resulting in hemolytic anemia. In humans, PK deficiency is the most prevalent glycolytic enzyme defect, which is responsible for hereditary hemolytic anemia [4,5].

We have previously established SLC3 [6], a line of Friend erythroleukemic cells from the *Pk-1*^{tlc} mouse [7], which has chronic hemolytic anemia with marked splenomegaly due to a missense mutation of the murine *Pklr* gene [8]. SLC3 showed spontaneous apoptosis during routine passage and in vitro erythroid differentiation by butyrate exacerbated apoptosis of SLC3 [6]. Recently, we examined the spleen of a subject with severe PK deficiency [9], and discovered enhanced extramedullary hematopoiesis as well as apoptotic erythroid cells. Enhanced apoptosis

Offprint requests to: Hitoshi Kanno, M.D. Ph.D., Department of Transfusion Medicine and Cell Processing, Tokyo Women's Medical University, Tokyo 162-8666, Japan.

0301-472X/07 $–see front matter.
doi: 10.1016/j.exphem.2007.05.005

was also identified in TER119-positive erythroid cells isolated from *Pk-1*^{slc} mice [10]. These results provide evidence that the metabolic disturbances in PK deficiency affect not only the survival of RBCs but also the maturation of erythroid progenitors, which results in apoptosis.

In this study, we examined whether Friend erythroleukemic cell lines showed apoptosis when glycolysis was inhibited. To evaluate whether overexpression of the normal R-PK gene ameliorated apoptosis, we established stable transfectants of SLC3 and compared their apoptotic characteristics and transcriptional profiles with parental SLC3. We present here several pieces of evidence, revealing the biological significance of R-PK to suppress oxidative stress during erythroid differentiation.

Materials and methods

Cell culture and flow cytometric analysis

Friend erythroleukemic cell lines SLC3 and CBA2 have been described previously [6]. Both cell lines are maintained in Iscove's modified Dulbecco's medium (Invitrogen, Carlsbad, CA, USA) supplemented with 10% heat-inactivated fetal calf serum, 20 μM 2-mercaptoethanol, and a mixture of penicillin-streptomycin (Sigma-Aldrich, St Louis, MO, USA).

To evaluate the adverse effects of glycolytic inhibition, cells were cultured in either glucose-free RPMI-1640 (Invitrogen) or RPMI-1640 with 2-deoxyglucose (2-DG) at final concentrations of 0.1, 1, and 10 mM. Iscove's modified Dulbecco's medium containing 110 mg/L sodium pyruvate, and RPMI-1640 containing no pyruvate.

Flow cytometric analysis was performed by EPICS XL and analyzed with software, EXPO32 ADC (Beckman-Coulter, Fullerton, CA, USA). Annexin V-Alexa568 and rhodamine 123 were obtained from Roche Diagnostics (Basel, Switzerland) and Sigma, respectively. To examine the effect of N-acetyl-L-cysteine upon apoptosis, we preincubated cells in RPMI-1640 supplemented with 10 mM N-acetyl-L-cysteine for 12 hours, followed by 12- to 24-hour incubation with RPMI-1640.

Establishment of stable transfectants expressing normal R-PK in SLC3 cells

We constructed a human R-PK cDNA expression plasmid vector in erythroid cells. A 1.7-kb fragment covering the entire coding region of human R-PK cDNA [11] was introduced into *Kpn*I-*Eco*RV sites of pcDNA3.1 (Invitrogen). Plasmid DNA was purified with an EndoFree Maxi DNA purification kit (Qiagen, Hilden, Germany). Transfection was done with Effectene Transfection Reagent (Qiagen) as indicated by the manufacturer. Transfected cells were selected using G418 (400 μg/mL).

RT-PCR, Western blotting, and enzyme assay

Total cellular RNA was extracted with an RNeasy purification kit (Qiagen), and 2 μg RNA was reverse-transcribed (RT) at 42°C for 90 minutes with 50 pmole oligo (dT)17 primer, 0.5 U/μL cloned RNase inhibitor (Takara Bio, Shiga, Japan), 10 mM dithiothreitol, 1 mM deoxyribonucleoside triphosphate, and 50 U Expand Reverse Transcriptase (Roche Diagnostics). Aliquots (1/10) were subjected to PCR using primer pairs specifically amplified with human and murine R-PK cDNA, hRPK-F (5′-TGGCCCAGC CTACCCTTGTA-3′)/hRPK-R (5′-CTTAAAGGTGGGGCTTTG GA-3′) and mRPK-F (5′-GCAGATGATGTGGACCGAAG-3′)/ mRPK-R (5′-CTAGATGGCAGATGTGGGACTA-3′), respectively. The reaction mixtures were subjected to 40 cycles of amplification consisting of 94°C for 20 seconds, 60°C for 10 seconds, and 72°C for 10 seconds for hRPK and 94°C for 20 seconds, 60°C for 20 seconds, and 72°C for 20 seconds for mRPK in a GeneAmp PCR system 2400 (Roche Diagnostics, Switzerland), and separated using 2% agarose gel electrophoresis.

For Western blot analysis, cells were harvested, followed by washing with phosphate-buffered saline twice. Following three-times freezing and thawing in extraction buffer (10 mM Tris/HCl, pH 8.0, 10 mM $MgCl_2$, 0.003% 2-mercaptoethanol, 0.02 mM ethylenediamine tetraacetic acid), cell extracts were obtained for Western blot analysis. Protein assays were performed by the method of Bradford using a commercial kit (Bio-Rad Laboratories, Hercules, CA, USA).Western blot analysis was conducted using anti-rat L-PK (kindly provided Tamio Noguchi, Nagoya University) and ECL advance Western Blotting Detection Kit (Amersham Biosciences, Buckinghamshire, UK).

PK and lactate dehydrogenase (LDH) activity was measured, as described [12].

Microarray analysis

To prepare high-quality total cellular RNA for the GeneChip assay, RNA was extracted with modified protocols using the TRIzol LS (Invitrogen) and RNeasy purification kit (Qiagen). Briefly, cells were harvested with no washing step, and immediately homogenized with the RLT buffer. The lysate was then mixed with 3 volumes of the TRIzol LS. After a 10-minute incubation at room temperature, the sample solution was mixed with an equal volume of chloroform. The sample was centrifuged at 10,000*g* for 15 minutes at 4°C, and then the upper aqueous phase was transferred to a fresh tube. After mixing with an equal volume of 70% ethanol, the sample was incubated for 10 minutes at room temperature. Without any flash step, the sample solution was transferred to the RNeasy column, and then processed by the manufacturer recommended protocol.

To normalize the variation in data based on the cell count, we used *Bacillus subtilis* RNA for an external standard signal, which was added to the cell lysate in proportion to the sample's DNA contents [13]. Ten microliters of cell lysate was provided for DNA quantification using Picogreen (Invitrogen). GeneChip (Affymetrix, Santa Clara, CA, USA) analysis was carried out according to the Affymetrix-recommended protocols. Processed RNA was hybridized to the Affymetrix Murine Genome 430A arrays (22960 probe sets). Signal values were calculated from scanned images by the Affymetrix Microarray Operation System (GCOS). The cell sample was pooled from six culture dishes at each condition and one GeneChip was used per one pooled sample.

Data analysis

Data were normalized by an original program (SCal), which processes data in proportional conversion based on the DNA content of each biosample [13]. This DNA content-based normalization method improves the measurement accuracy of GeneChip. For example, a series of samples was measured by quantitative PCR and Affymetrix GeneChip microarrays using this method, and the results showed up to 90% concordance [13].

To identify differentially expressed genes, we used an empirical threshold calculated by an original algorithm (Fx). The Fx threshold is based on the signal intensity level and is calculated as follows: $Y = X \cdot (1 + RC^{(w\text{-}\log X)})$ and $Y = X \cdot (1 + C^{(w\text{-}\log X)})^{-1}$ (Fx1 and Fx2 respectively; C and w are constant parameters reflecting actual measurement data by GeneChip hybridized with the standard sample). C and w were set to 3.0 and 2.5, respectively, which was equivalent to $p < 0.02$. In the scatter plot, the spots above the Fx1 line were evaluated as upregulated, and the spots below the Fx2 line were evaluated as downregulated.

Results

SLC3 is more susceptible than the control to apoptosis due to glycolytic inactivation

Figure 1 shows flow cytometric analysis using annexin V (horizontal axis) and rhodamine 123 (vertical axis) to examine the effects of glycolysis inhibition on Friend leukemic cells with or without R-PK mutation. SLC3 showed spontaneous apoptosis during routine passage, and apoptosis preceded mitochondrial dysfunction in the R-PK–deficient erythroleukemia cells as reported previously [6]. The result showed that a part of apoptotic cells kept similar mitochondrial transmembrane potentials and that SLC3 were much more susceptible to glucose deprivation as well as 2-DG.

Overexpression of wild-type R-PK decreases apoptosis of SLC3

In order to evaluate how wild-type R-PK rescues apoptotic phenotypes, we established two stable transfectants of SLC3 with overexpression of the human R-PK cDNA. Figure 2 shows RT-PCR and Western blot analysis of a parental SLC3 and SLC3-hRPK.Hi (hRPK.Hi) and SLC3-hRPK.Lo (hRPK.Lo). As shown in Figure 2A, the expression level of the transgene was higher in hRPK.Hi than hRPK.Lo. Overexpression of human R-PK suppressed endogenous R-PK expression as observed in the lane of hRPK.Hi.

Enzymatic analysis of transfectants revealed that PK activities of hRPK.Lo and Hi were 17.2 and 24.2 IU/mg protein, respectively. The PK activity of hRPK.Hi was almost comparable to parental SLC3, 23.5 IU/mg protein. It should be noted that endogenous LDH activity was decreased by transgene expression, leading to a PK/LDH ratio increase from 0.4 (SLC3) to 0.48 (hRPK.Lo) and 0.6 (hRPK.Hi).

We evaluated apoptosis of the two transfectants by cell cycle analysis. Figure 2C shows that the expression of wild-type R-PK decreased the number of cells at the sub-G_0/G_1 stage. While hRPK.Lo showed almost the same number of sub-G_0/G_1 cells (55.5%) as SLC3 (57.4%), only 19.3% of hRPK.Hi were arrested at the sub G_1-stage. Because apoptotic cells were rescued from apoptosis in an R-PK expression level-dependent manner, it is most likely that R-PK activity is required to suppress apoptosis of erythroid cells.

Microarray analysis elucidates the differential expression of genes involved in reactive oxygen species removal, cell cycle, and apoptosis

Gene expression profiles between the two transfectants and the parental SLC3 cell line were analyzed by DNA microarray analysis. After exchanging culture medium, SLC3, hRPK.Lo, and Hi were sampled at 24 and 67 hours, which were the phase of reentry into cell cycling and of subconfluence, respectively. Transgene expression upregulated only about 2% (469 probe sets) of genes, whereas approximately 25% (5754 probe sets) of genes were downregulated both in hRPK.Hi and hRPK.Lo at 24 and/or 67hours. As shown in Figure 3B, major categories of the downregulated genes involved the cell cycle, development, and apoptosis. Proapoptotic genes including *Bad*, *Bnip3*, and *Bnip3l*, as well as *Casp 2, 6, 7,* and *8* were downregulated (Figs. 3A and 4).

Genes of key glycolytic enzymes such as hexokinase-2 (*Hk2*), phosphofructokinase (*Pfkl*), phosphoglycerate kinase (*Pgkl*), and PK (*Pklr*) were downregulated, and expression levels were characteristically decreased after 67 hours of transfection, suggesting that suppression requires protein synthesis.

It should be noted that genes for antioxidant protein, such as peroxiredoxin 1 (*Prdx1*) and related genes, such as catalase (*Cat*), thioredoxin reductase 1 (*Txnrd1*), and glutaredoxin 1 (*Glrx1*), which have a role in the modulation of oxidative stress, are also downregulated. As for *Prdx2*, expression change by the transgene was not evident. Intracellular reactive oxygen species (ROS) are known to cause DNA damage, inducing the expression of DNA repair genes. In this experiment, expressions of genes involved in DNA repair were decreased, including *Brca1*, *Brca2*, and *Rad51*.

PK gene mutation and glycolytic inhibition by 2-DG augment intracellular ROS

We examined intracellular ROS in SLC cells and control CBA2 cells by 2′,7′-dichlorofluorescin-diacetate (DCFH-DA), an indicator of the intracellular formation of hydrogen peroxide and free radicals. Nonfluorescent DCFH-DA turns into DCFH (2′,7′-dichlorofluorescin) in the presence of hydrogen peroxide, and then DCFH is quickly photo-oxidized to fluorescent DCF (2′,7′-dichlorofluorescein).

Figure 5A shows that SLC3 is hypersensitive to a glycolytic inhibitor, 2-DG, producing intracellular DCF by adding 1 mM 2-DG. In contrast, control CBA2 cells do not produce DCF even at 10 mM 2-DG for 30 minutes.

Reduced glutathione (GSH) is an important antioxidant in erythrocytes. GSH is produced by a two-step enzymatic reaction involving γ-glutamylcystein synthetase and glutathione synthetase (GSH-S). Apoptosis induced either by the glycolytic gene mutation (SLC3) or the glycolytic inhibitor (CBA with 2-DG) was suppressed by preincubation with the glutathione precursor, NAC (Fig. 5B). Finally, the

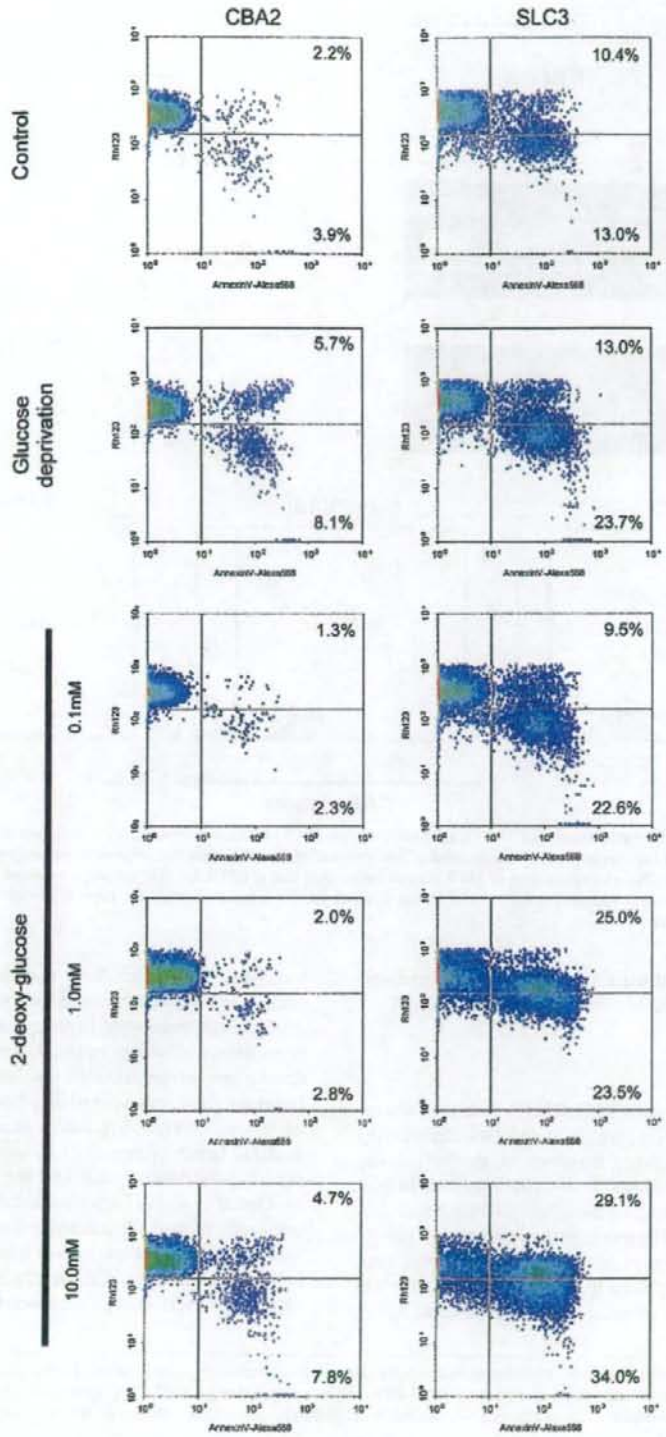
CBA2
SLC3
Control
Glucose deprivation
2-deoxy-glucose
0.1mM
1.0mM
10.0mM
2.2%
3.9%
10.4%
13.0%
5.7%
8.1%
13.0%
23.7%
1.3%
2.3%
9.5%
22.6%
2.0%
2.8%
25.0%
23.5%
4.7%
7.8%
29.1%
34.0%

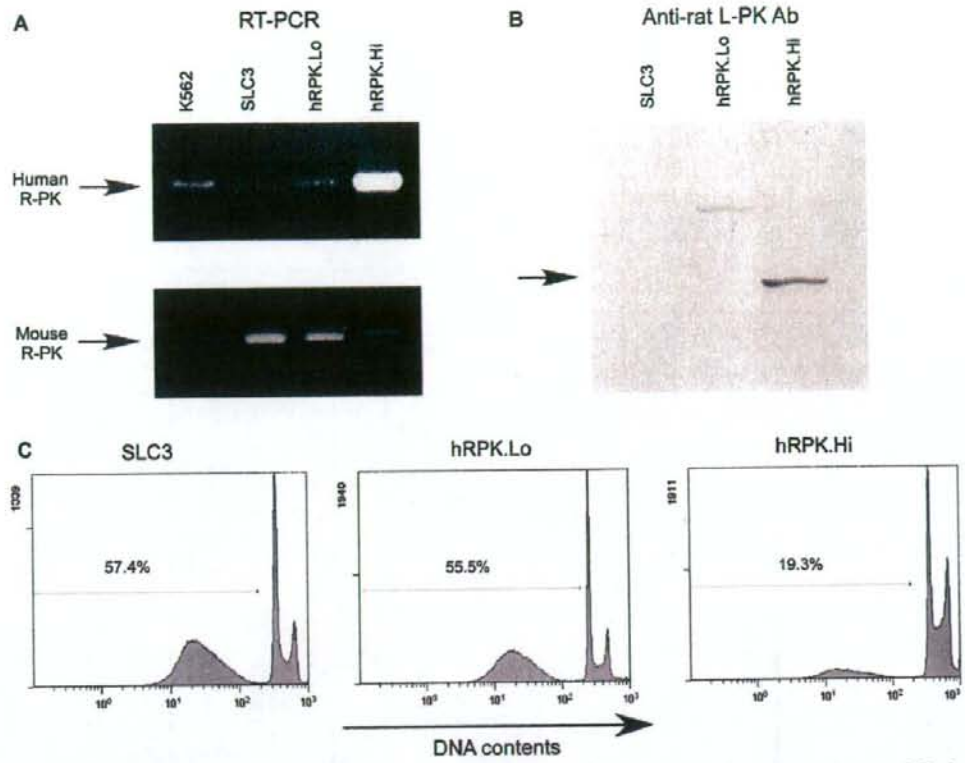

Figure 2. Establishment of the transfectants, SLC3-hRPK.Hi (hRPK.Hi) and SLC3.hRPK.Lo (hRPK.Lo), by introducing the human red blood cell type-pyruvate kinase (R-PK) gene into murine R-PK–deficient cells. Transgene-expression was confirmed by reverse transcriptase polymerase chain reaction (**A**) and Western blotting (**B**). The expression level of hRPK.Hi was higher than that of hRPK.Lo. (**C**) Apoptosis induction in the PK-deficient cells and transfectants. Transfected human R-PK recovered the glycolytic function and showed reduced spontaneous apoptotic changes. The numbers in figures represent the apoptotic change ratio.

forced overexpression of the PK gene reduced intracellular ROS in an expression-level dependent manner (Fig. 5C).

Discussion

Overexpression of human R-PK in SLC3 results in the reduction of apoptotic cells (Fig. 2C), and DNA microarray analysis showed that genes involved in the cell cycle, DNA repair, and antioxidants were downregulated. In general, gene expression levels of transfectants were lower than that of SLC3 (Fig. 3). However, aberrant apoptosis and invalid cell proliferation were restrained in the transfectants. These observations suggested that the cellular activity was not suppressed but was reverted to the normal level by the transgene. It is most likely that the candidate genes suppressed in transfectants were induced in R-PK mutant cells.

Although there were several candidate genes attributing to apoptosis-induction in SLC3, it was still unclear whether these genes were associated with each other or independent. However, there was a possibility that a signal cross-talk phenomenon occurred [14]. *Bad*, a gene encoding a member of the Bcl2-family proapoptotic molecules in mitochondria was significantly downregulated by the transgene (Figs. 3A and 4). Danial et al. [15] reported that *Bad*, BCL2-antagonist of cell death, formed a functional holoenzyme complex together with several molecules, such as glucokinase (hexokinase-4) in liver mitochondria, and contributed to apoptosis induction by glucose deprivation. Our observation suggested that *Bad*

Figure 1. Apoptosis induced by glycolytic inhibition in erythroid cell lines. Glucose deprivation or exposure to 2-deoxyglucose inhibits glycolysis and finally causes apoptosis. The red blood cell type-pyruvate kinase (R-PK)–deficient erythroid cell line (SLC3) is more susceptible than wild-type cells (CBA2) in these conditions. The horizontal axis shows AnnexinV-Arexa568 (= apoptotic change) and the vertical axis shows Rhodamin123 fluorescence (= mitochondrial membrane potential).

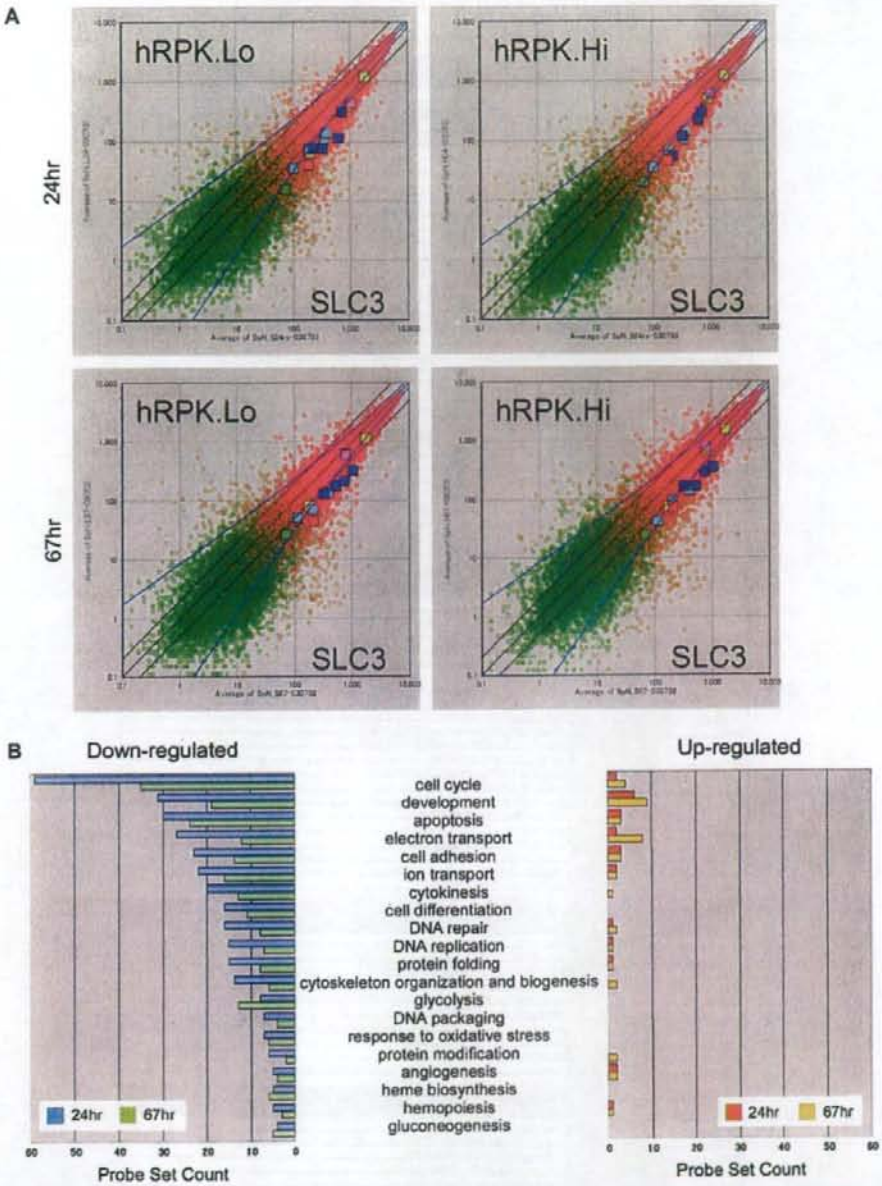

Figure 3. Genome-wide expression analysis of the glycolysis defect. Analysis was performed using the Affymetrix GeneChip Mouse Expression Array 430A, which contains about 20,000 genes. (**A**) Scatter plot between SLC3 and hRPK transfectants at 24 or 67 hours. The open circle shows the expression level of every probe set. The color shows these probabilities provided by the Affymetrix GeneChip Operation System: red means good and green means poor. The colored squares show *Bad* (red), *Bnip3* and *Bnip3l* (blue), *hif1a* (green), *Brca1* and *Brca2* (aqua), *Prdx1* (pink) and *Txnl1* (yellow), respectively. The black lines show twofold, onefold, and 0.5-fold, respectively, and the blue lines show the empirical threshold level. (**B**) The categorized aggregate graph. All probe sets were categorized by the Biological Process Ontology keywords provided by the Gene Ontology project (http://www.geneontology.org/). Up- or downregulation was determined by the spot location in the scatter plotting. Compared with the empirical threshold lines, the upper spots show upregulated genes and the lower spots show downregulated genes.

A

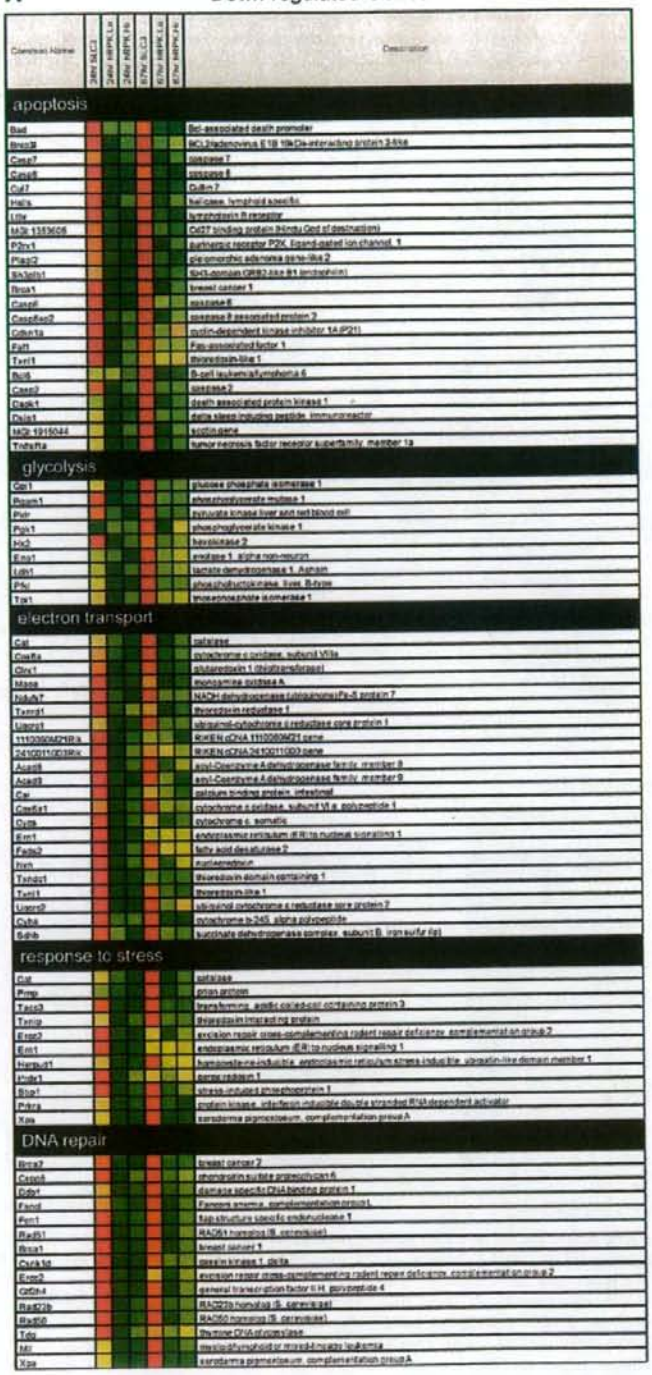
Down-regulated Genes
Description
apoptosis
Bad
Bcl2l1
Casp7
Casp8
Cul7
Hells
Lilr
Mib 1353605
P2rx1
Plagl2
Sh3glb1
Brca1
Casp6
Caspfap2
Cdkn1a
Faf1
Txnl1
Bcl6
Casp2
Dapk1
Dsls1
Mgc 1915044
Tnfrsf1a
glycolysis
Gbt1
Pgam1
Pklr
Pgk1
Hk2
Eno1
Ldh1
Pfkl
Tpi1
electron transport
Cat
Cox6a
Clns1
Masa
Ndufs7
Txnrd1
Uqcrc1
1110008M21Rik
2410011D03Rik
Aldh8
Aldh9
Cav
Cox6a1
Cycs
Ern1
Fads2
Hrh
Txndc1
Txnl1
Uqcrc2
Cyba
Sdhb
response to stress
Cat
Prnp
Tacc3
Txnip
Ercc2
Ern1
Herpud1
Hspb1
Stip1
Prkra
Xpa
DNA repair
Brca2
Casp8
Ddb1
Fancd
Fen1
Rad51
Brca1
Cdkn1d
Ercc2
Gtf2h4
Rad23b
Rad50
Tdg
Mll
Xpa

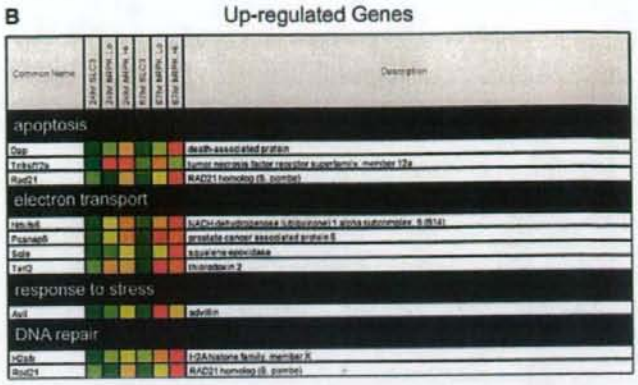

Figure 4. *Continued*

could be involved in the apoptosis induced by glycolysis defect in erythroid cells as well as in the liver.

The genes of apoptosis-inducers related to hypoxia such as *Bnip3* and *Bnip3l*, which are known as inducible genes by hypoxia-inducible factor-1α, were inactivated markedly by the forced expression of the wild-type R-PK gene. Although the extent of downregulation was smaller than for *Bnip3*, *Bnip3l* showed a significant decrease of expression by the transgene (Fig. 3A). Moreover, the downregulation was more obvious at 24 hours, suggesting that these genes may contribute to the initial response caused by a glycolytic defect. These observations strongly suggested that the apoptosis induction by the glycolysis disorder was executed by the *Bnip3-Bnip3l* signal.

It is noticeable that several genes important for responding to oxidative stress are upregulated, suggesting that R-PK deficiency might account for intracellular ROS production. This speculation is supported by the following experimental observations: Firstly, SLC3 cells were more sensitive to glycolytic inhibitions such as glucose deprivation and supplementation with 2-DG (Fig. 1), and these conditions induced ROS production detected by DCFH-DA (Fig. 5A). Apoptotic changes induced by 2-DG were partly rescued by preincubation with the glutathione precursor (Fig. 5B). Finally, transgene expression reduced intracellular ROS in an expression-level–dependent manner (Fig. 5C).

Glycolytic disorders may cause cellular conditions similar to those of hypoxia. Shim et al. [16] reported that induction of the LDH-A gene by c-Myc was advantageous to transformed cells that exist under hypoxic conditions [15]. However, glucose deprivation induces the extensive apoptosis of cells overexpressing c-Myc. Overexpression of LDH-A alone in fibroblasts is sufficient to sensitize cells to this glucose deprivation-induced apoptosis. They proposed a hypothesis that LDH-A was a downstream target of c-Myc that mediates this unique apoptotic phenotype. We noticed that pyruvate was the final product as well as the substrate of the PK and LDH reaction, respectively. Both LDH hyperactivity and PK deficiency may cause the depletion of intracellular pyruvate, suggesting that pyruvate has an important role in preventing apoptosis.

Several studies have revealed that pyruvate acts as an antioxidant and that PK has a protective role against oxidative stress in this respect. Brand et al. [17] reported that proliferating thymocytes mainly depend on energy derived from aerobic glycolysis, and that their sensitivity to 12-myristate 13-acetate–induced ROS production is much lower than that of resting thymocytes, which produce ATP mainly through oxidative phosphorylation. They suggested that pyruvate functions as an ROS scavenger, because the incubation of proliferating thymocytes with pyruvate reduced ROS formation.

The PK-overexpressing neuronal cells could attenuate oxidative stress and maintain cell viability [18]. Lee et al. [19] showed that hydrogen peroxide depleted intracellular GSH in human umbilical vein endothelial cells, and that was prevented by pyruvate but not by L-lactate or aminooxyacetate. The activation of caspases was strongly inhibited by pyruvate, but markedly enhanced by L-lactate and aminooxyacetate, implicating the redox-related antiapoptotic mechanisms of pyruvate. Myocardial ischemia-reperfusion

Figure 4. Representative list of the genes affected by the functional recovery of glycolysis. Genome-wide expression analysis was performed using Affymetrix GeneChip Mouse Expression Array 430A, which contains about 20,000 genes. In the comparison among hRPK.Hi, hRPK.Lo, and SLC3, about 6000 genes were downregulated and about 500 genes were upregulated by the functional recovery of glycolysis at 24 and/or 67 hours after regular passage. These lists contain the affected genes related to apoptosis and/or the oxidative stress response.

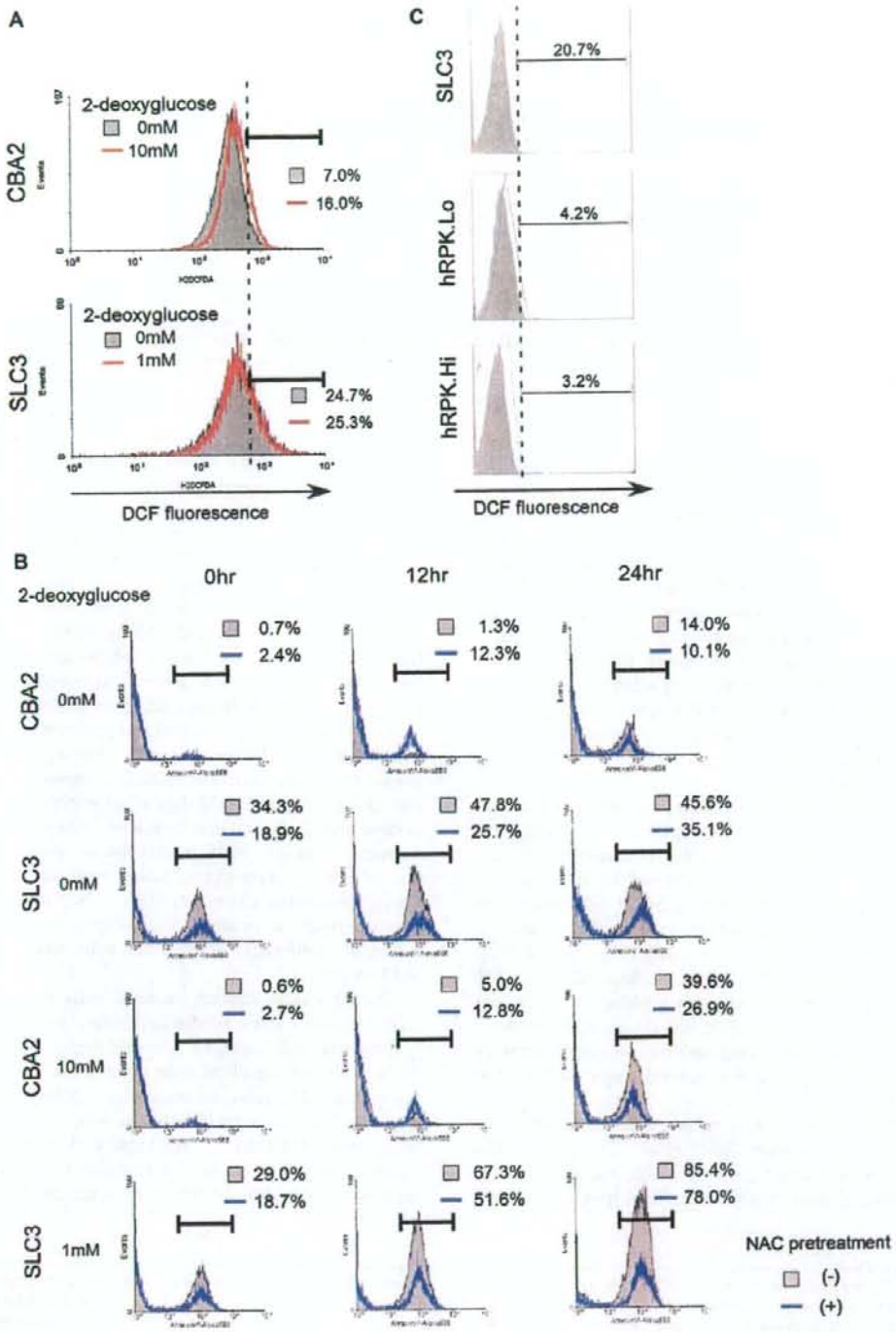
A
CBA2
2-deoxyglucose
0mM
10mM
7.0%
16.0%
SLC3
2-deoxyglucose
0mM
1mM
24.7%
25.3%
DCF fluorescence
C
SLC3
20.7%
hRPK.Lo
4.2%
hRPK.Hi
3.2%
DCF fluorescence
B
2-deoxyglucose
0hr
12hr
24hr
CBA2 0mM
0.7%
2.4%
1.3%
12.3%
14.0%
10.1%
SLC3 0mM
34.3%
18.9%
47.8%
25.7%
45.6%
35.1%
CBA2 10mM
0.6%
2.7%
5.0%
12.8%
39.6%
26.9%
SLC3 1mM
29.0%
18.7%
67.3%
51.6%
85.4%
78.0%
NAC pretreatment
(-)
(+)

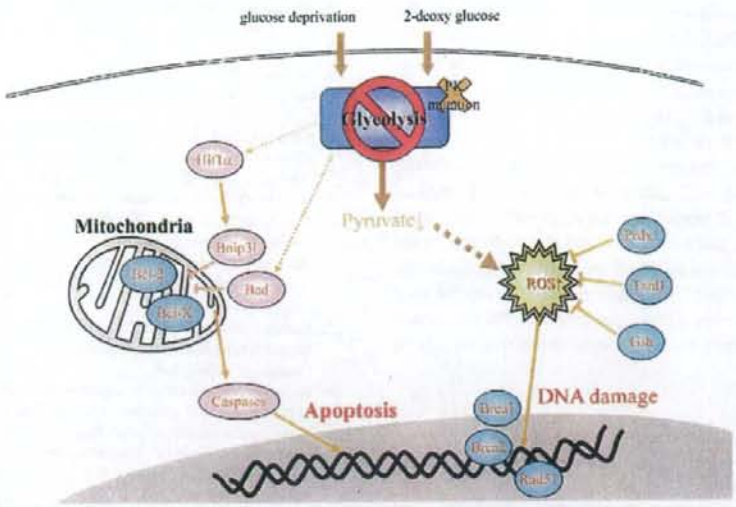

Figure 6. Glycolytic defect causes oxidative stress and hypoxia-like signal activation. Pyruvate, which is final metabolic product of the glycolytic pathway, acts as an antioxidant. Therefore, glycolytic defect elevates intracellular reactive oxygen species (ROS) and causes cellular damage, such as DNA damage and lipid oxidation. At the same time, glycolytic defect is most likely to activate signal transduction through hypoxia-inducible factor-1α (HIF-1α). These cellular responses could be accountable for the apoptosis induced by glycolytic defect.

is reported to be associated with bursts of ROS, such as superoxide radicals, and cardiac superoxide formation can be inhibited by pyruvate [20]. Thus cytotoxicities due to cardiac ischemia-reperfusion ROS can be alleviated by redox reactants such as pyruvate. These results support our present data, which showed that a mutation of the PK gene as well as inhibition of glycolysis by 2-DG augmented intracellular ROS of erythroid cells, leading to apoptosis. Introduction of the wild-type PK gene into SLC3 cells partly reduced ROS and apoptosis (Figs. 2C and 6C).

In human RBC, the most important antioxidant is GSH. Mutations of enzymes involving the synthesis and reduction of GSH, such as γ-glutamylcystein synthetase, GSH-S, glutathione reductase, and glucose-6-phosphate dehydrogenase account for the shortened RBC survival [1,21]. Recently, Neumann et al. [22] and Lee et al. [23] reported the essential roles of both peroxiredoxin (Prdx) 1 and 2 in RBC protection from oxidative stress. The hemolytic anemia of mice with targeted inactivation of *Prdx1* is characterized by an increase in erythrocyte reactive oxygen species, leading to protein oxidation and Heinz body formation. Similarly, the *Prdx2* knockout mice had Heinz body-positive hemolytic anemia with splenomegaly. The dense RBC fractions contained markedly higher levels of ROS. These studies highlighted a pivotal role of *Prdx* as a scavenger of hydrogen peroxide in RBC. *Prdx1* may be concerned with the initial response to glycolytic deficiency, because the gene expression in SLC3 was higher than that in transfectants only at 24 hours (Fig. 3A). The mechanisms responsible for upregulation of *Prdx1* and similar antioxidant enzymes in SLC3 remain to be elucidated.

It is most likely that the main pathogenesis of PK deficiency is decreased ATP production due to impaired glycolysis, resulting in the premature destruction of RBC in the reticuloendothelial system, i.e., extravascular hemolysis. In most cases, hemolysis is partly compensated by enhanced erythropoiesis. We have previously shown that the numbers of hematopoietic progenitors including colony-forming unit (CFU)-erythroid, CFU-granulocyte macrophage, burst-forming unit-erythroid, and CFU-granulocyte-erythrocyte monocyte-megakaryocyte were increased in *Pk-1*^{stc} mice [10]. The proliferation of erythroid progenitors might require

Figure 5. The oxidative stress pathway might play some role in the apoptosis induced by glycolytic disorder. (A) The SLC3 cells produce 2',7'-dichlorofluorescein (DCF) continuously with and without 2-deoxyglucose (2-DG) due to the red blood cell type-pyruvate kinase (R-PK) defect. The control CBA2 cells produce DCF with 10 mM 2-DG for 30 minutes. The gray area shows the nontreated group and the red line shows the treated group with 2-DG. The horizontal axis shows the fluorescence intensity of the DCF. (B) The apoptosis induced by glycolytic defect or by glycolysis inhibitor was suppressed by the preincubation with the glutathione precursor, N-acetyl-cysteine (NAC). The gray area shows the nonpretreated group and the blue line shows the pretreated group with NAC. The horizontal axis shows the fluorescence intensity of the Annexin V-Alexa568.

activation of glycolysis in order to suppress intracellular ROS. Therefore, R-PK deficiency becomes a serious problem for erythroid cells to avoid apoptosis. In summary, we concluded that the premature destruction of RBC as well as apoptosis of erythroid progenitors accounts for the pathogenesis of R-PK deficiency.

Although most severe cases die either in utero or during the neonatal period [24,25], there is no curative therapy of PK deficiency except hematopoietic stem cell transplantation [26] at present. Because hematopoietic stem cell transplantation may accompany life-threatening complications, a safer treatment should be considered. Studies on the apoptotic induction of erythroid progenitors in R-PK deficiency may be useful for the identification of molecular targets of causal treatment.

Acknowledgments

We are indebted to Takako Hamada and Miyuki Yuda for their excellent technical assistance. This work was supported in part by a Grant-in-Aid for Scientific Research from the Japan Society of the Promotion of Science (project nos. 14570131 and 16590254), and also by a Scientific Research Grant from the Ministry of Health, Labor and Welfare (H15-kagaku-002, H18-kagaku-ippan-001), Japan.

References

1. Hirono A, Kanno H, Miwa S, Beutler E. Pyruvate kinase deficiency and other enzymopathies of the erythrocyte. In: Scriver CR, Beaudet AL, Sly WS, Valle D, eds. The Metabolic & Molecular Bases of Inherited Disease. 8th ed. New York: McGraw-Hill; 2001. p. 4637–4664.
2. Takegawa S, Fujii H, Miwa S. Change of pyruvate kinase isozymes from M2- to L-type during development of the RBC. Br J Haematol. 1983;54:467–474.
3. Max-Audit I, Kechemir D, Mitjavila MT, Vainchenker W, Rotten D, Rosa R. Pyruvate kinase synthesis and degradation by normal and pathologic cells during erythroid maturation. Blood. 1988;72: 1039–1044.
4. Tanaka KR, Zerez CR. RBC enzymopathies of the glycolytic pathway. Semin Hematol. 1990;27:165–185.
5. Zanella A, Fermo E, Bianchi P, Valentini G. RBC pyruvate kinase deficiency: molecular and clinical aspects. Br J Haematol. 2005;130: 11–25.
6. Aisaki K, Kanno H, Oyaizu N, Hara Y, Miwa S, Ikawa Y. Apoptotic changes precede mitochondrial dysfunction in red cell-type pyruvate kinase mutant mouse erythroleukemia cell lines. Jpn J Cancer Res. 1999;90:171–179.
7. Morimoto M, Kanno H, Asai H, et al. Pyruvate kinase deficiency of mice associated with nonspherocytic hemolytic anemia and cure of the anemia by marrow transplantation without host irradiation. Blood. 1995;86:4323–4330.
8. Kanno H, Morimoto M, Fujii H, et al. Primary structure of murine red blood cell-type pyruvate kinase (PK) and molecular characterization of PK deficiency identified in the CBA strain. Blood. 1995;86: 3205–3210.
9. Aizawa S, Kohdera U, Hiramoto M, et al. Ineffective erythropoiesis in the spleen of a patient with pyruvate kinase deficiency. Am J Hematol. 2003;74:68–72.
10. Aizawa S, Harada T, Kanbe E, et al. Ineffective erythropoiesis in mutant mice with deficient pyruvate kinase activity. Exp Hematol. 2005; 33:1292–1298.
11. Kanno H, Fujii H, Hirono A, Miwa S. cDNA cloning of human R-type pyruvate kinase and identification of a single amino acid substitution (Thr384→Met) affecting enzymatic stability in a pyruvate kinase variant (PK Tokyo) associated with hereditary hemolytic anemia. Proc Natl Acad Sci U S A. 1991;88:8218–8221.
12. Beutler E, Blume KG, Kaplan JC, Loehr GW, Ramot B, Valentine WN. International Committee for Standardization in Haematology: recommended methods for red cell enzyme analysis. Br J Haematol. 1977;35:331–340.
13. Kanno J, Aisaki K, Igarashi K, et al. "Per cell" normalization method for mRNA measurement by quantitative PCR and microarrays. BMC Genomics. 2006;29:64.
14. Krones A, Jungermann K, Kietzmann T. Cross-talk between the signals hypoxia and glucose at the glucose response element of the L-type pyruvate kinase gene. Endocrinology. 2001;142:2707–2718.
15. Danial NN, Gramm CF, Scorrano L, et al. BAD and glucokinase reside in a mitochondrial complex that integrates glycolysis and apoptosis. Nature. 2003;424:952–956.
16. Shim H, Chun YS, Lewis BC, Dang CV. A unique glucose-dependent apoptotic pathway induced by c-Myc. Proc Natl Acad Sci U S A. 1998;95:1511–1516.
17. Brand K, Netzker R, Aulwurm U, et al. Control of thymocyte proliferation via redox-regulated expression of glycolytic genes. Redox Rep. 2000;5:52–54.
18. Shimizu T, Uehara T, Nomura Y. Possible involvement of pyruvate kinase in acquisition of tolerance to hypoxic stress in glial cells. J Neurochem. 2004;91:167–175.
19. Lee YJ, Kang IJ, Bunger R, Kang YH. Mechanisms of pyruvate inhibition of oxidant-induced apoptosis in human endothelial cells. Microvasc Res. 2003;66:91–101.
20. Basing E, Summer O, Schemer M, Bunger R. Antioxidant pyruvate inhibits cardiac formation of reactive oxygen species through changes in redox state. Am J Physiol Heart Circ Physiol. 2000;279:H2431–H2438.
21. Luzzatto L, Mehta A, Vulliamy T. Glucose 6-phosphate dehydrogenase. In: Scriver CR, Beaudet AL, Sly WS, Valle D, eds. The Metabolic & Molecular Bases of Inherited Disease. 8th ed.. New York: McGraw-Hill; 2001. p. 4517–4554.
22. Neumann CA, Krause DS, Carman CV, et al. Essential role for the peroxiredoxin Prdx1 in erythrocyte antioxidant defense and tumour suppression. Nature. 2003;424:561–565.
23. Lee TH, Kim SU, Yu SL, et al. Peroxiredoxin II is essential for sustaining life span of erythrocytes in mice. Blood. 2003;101:5033–5038.
24. Ferreira P, Morais L, Costa R, et al. Hydrops fetalis associated with erythrocyte pyruvate kinase deficiency. Eur J Pediatr. 2000;159: 481–482.
25. Bowman HS, McKusick VA, Dronamraju KR. Pyruvate kinase deficient hemolytic anemia in an Amish isolate. Am J Hum Genet. 1965;17:1–8.
26. Tanphaichitr VS, Suvatte V, Issaragrisil S, et al. Successful bone marrow transplantation in a child with red blood cell pyruvate kinase deficiency. Bone Marrow Transplant. 2000;26:689–690.

Tbx6-mediated Notch signaling controls somite-specific *Mesp2* expression

Yukuto Yasuhiko*, Seiki Haraguchi†, Satoshi Kitajima*, Yu Takahashi*, Jun Kanno*, and Yumiko Saga‡§

*Cellular and Molecular Toxicology Division, National Institute of Health Sciences, Kamiyoga 1-18-1, Setagaya-ku, Tokyo 158-8501, Japan; †The Wellcome Trust/Cancer Research UK Gurdon Institute, University of Cambridge, Cambridge CB2 1QN, United Kingdom; and ‡Division of Mammalian Development, National Institute of Genetics, Mishima, Shizuoka 411-8540, Japan

Edited by Kathryn V. Anderson, Sloan–Kettering Institute, New York, NY, and approved January 10, 2006 (received for review September 21, 2005)

Mesp2 is a transcription factor that plays fundamental roles in somitogenesis, and its expression is strictly restricted to the anterior presomitic mesoderm just before segment border formation. The transcriptional on–off cycle is linked to the segmentation clock. In our current study, we show that a T-box transcription factor, Tbx6, is essential for *Mesp2* expression. Tbx6 directly binds to the *Mesp2* gene upstream region and mediates Notch signaling, and subsequent *Mesp2* transcription, in the anterior presomitic mesoderm. Our data therefore reveal that a mechanism, via Tbx6-dependent Notch signaling, acts on the transcriptional regulation of *Mesp2*. This finding uncovers an additional component of the interacting network of various signaling pathways that are involved in somitogenesis.

enhancer | transgenic mouse | RBPJκ | luciferase assay

Somitogenesis not only is an important morphogenic process that generates metameric structures in vertebrates, but it is also a intriguing model system for the study of the interactions among various signaling cascades that facilitate periodic pattern formation. The segmental boundary of each somite forms at the anterior end of the presomitic mesoderm (PSM) or unsegmented paraxial mesoderm, which is supplied from the primitive streak or tailbud at a later stage of development.

Notch signaling plays fundamental roles in segmental pattern formation by means of oscillating the activity in the tailbud, its forward movement through the PSM as traveling waves, and its stabilization at the anterior end of the PSM (1, 2). A segment border forms at the posterior limit of the stabilized stripe of Notch signaling activity (2). The oscillation of the Notch signals in the tailbud region is regulated by the transcription factor Hes7 (3), a glycosyltransferase Lunatic fringe (2), and by Wnt signaling (4). In contrast, the positioning of segment formation by a determination wavefront is thought to be defined by antagonistic interactions between gradients of Fgf signals from the posterior end (5) and retinoic acid (RA) from anterior end of the PSM (6). On the other hand, mutant analyses identified a T-box protein, Tbx6, as an indispensable component for correct PSM differentiation and segmentation (7). However, the direct molecular relationships between these factors have not yet been well characterized.

A basic helix–loop–helix transcription factor, Mesp2, has a crucial role both in somite segment border formation and in the establishment of the rostrocaudal patterning of each somite (8). *Mesp2* shows dynamic and periodical expression in the anterior PSM, which defines the positioning of the forming somite by suppressing Notch signaling, partly through the activation of *lunatic fringe* (2). Genetic analyses have revealed that *Mesp2* expression itself is controlled by Notch signaling, which indicates the presence of a complicated feedback circuitry (9, 10). However, the molecular mechanisms that control *Mesp2* expression remain largely unknown. In our present study, we show that Tbx6 directly binds to upstream elements of the *Mesp2* gene and is essential for the activation of *Mesp2* expression. Furthermore, we demonstrate that Notch signaling strongly enhances *Mesp2* activation by Tbx6, and we identify the sequences that are important for this enhancement. Hence, we identify a Tbx6-mediated Notch signaling pathway as a mechanism underlying the regulation of *Mesp2* expression.

Results and Discussion

Evolutionally Conserved Sites in the Upstream Region of the *Mesp2* Gene Promote Strong Reporter Activity in Forming Somites. The distinct expression patterns of *Mesp2* expression during somitogenesis are strictly regulated. As we previously reported (11), a transgenic approach has revealed that a 300-bp portion of the 5′-adjoining sequence of the *Mesp2* ORF induces lacZ reporter activity in forming somites. This finding reflects the *Mesp2* expression pattern in the anteriormost PSM, suggesting that this 5′ region includes cis elements that regulate PSM-specific *Mesp2* expression. We performed comparisons of the genomic sequences of mouse *Mesp2* and its putative ortholog in zebrafish, *mespb*, and identified five conserved sites (A–E) in this 300-bp segment (Fig. 1*A*). Each of these sites was then independently examined for enhancer properties by using a transgenic strategy. We previously showed that one of our transgenic constructs, *P2L-100*, containing sites D and E, which cover the 100 bp upstream of the *Mesp2* ATG start codon, did not activate the lacZ reporter gene (11). We thus concentrated our analysis on sites A–C in our current experiments by ligating them with the *P2L-100* construct. None of these three sites could individually promote lacZ reporter activity in somites (Fig. 1*B*). However, the combination of sites A and B (designated as "site A+B" hereafter) induced strong β-gal expression in the somite region (Fig. 1*B Left*). This result suggests that specific transcription factors required for somite-specific *Mesp2* expression may bind to site A+B.

Tbx6 Binds to Cis-Regulatory Elements of the *Mesp2* Gene and Activates Its Expression. To identify transcription factors that bind to the cis-regulatory elements of the *Mesp2* gene, we performed yeast one-hybrid screening. Using site A+B sequences as the "bait," we isolated a T-box transcription factor, Tbx6, as a candidate binding protein. T-box proteins have been shown to recognize and bind to nucleotide sequences of 10–11 bp in length that possess a conserved CACAC motif (12). Significantly, sites A, B, and D in the upstream sequences of the *Mesp2* gene contain this motif (Fig. 2*A*). EMSA subsequently revealed that FLAG-Tbx6 binds to both site B and site D, in addition to the T (Brachyury) binding consensus sequence (12) (Fig. 6*A*, which is published as supporting information on the PNAS web site). By using site B sequences as a probe for FLAG-Tbx6 binding, EMSA experiments produced two band shifts, a distinct band

Conflict of interest statement: No conflicts declared.

This paper was submitted directly (Track II) to the PNAS office.

Abbreviations: PSM, presomitic mesoderm; NICD, Notch intracellular domain; RA, retinoic acid.

§To whom correspondence should be addressed. E-mail: ysaga@lab.nig.ac.jp.

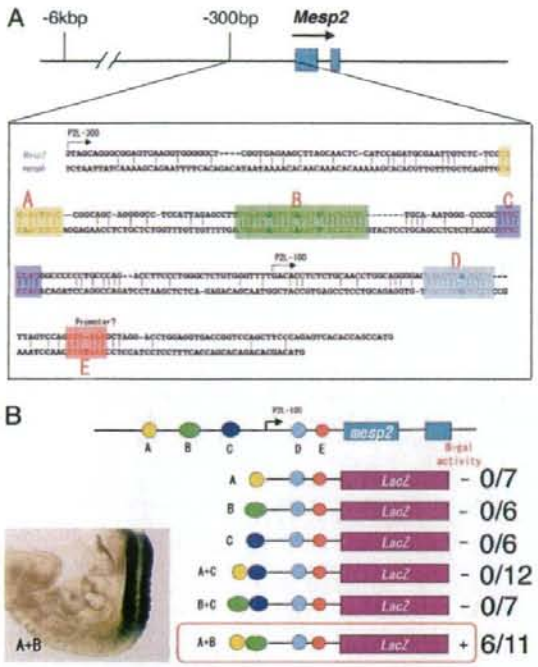

Fig. 1. Characterization of the *Mesp2* enhancer region. (*A*) Comparisons between the genomic sequences of mouse *Mesp2* and zebrafish *mespb* (an ortholog of mouse *Mesp2*) reveal five conserved sites in the 300-bp proximal promoter region. These conserved sites are denoted as A–E. The numbers above the genomic sequences indicate the base count from the ATG transcriptional start site of the *Mesp2* ORF. (*B*) Summary of the transient transgenic assay results with different combinations of conserved sites from the *Mesp2* upstream region (sites A–C). Each site was tested either alone or in combination with other sites for somite-specific enhancer activity. The presence (+) or absence (−) of β-gal activity and the incidence of this among transgene-positive embryos is shown schematically on the right of each reporter construct. The combination of site A and site B (shown as A+B) resulted in strong somite-specific enhancer activity (*Left*).

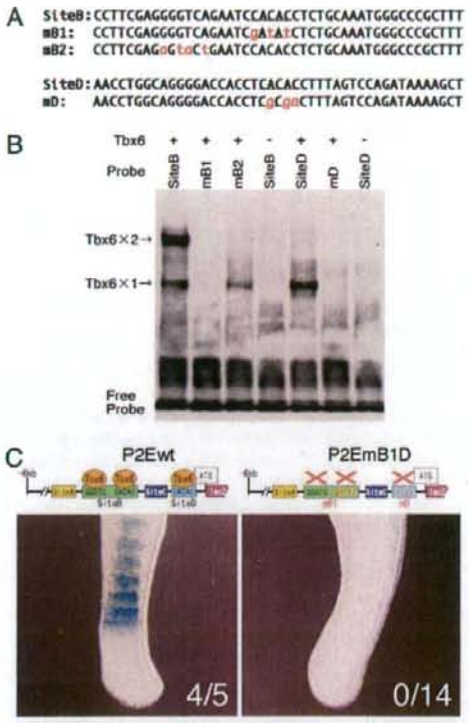

Fig. 2. Tbx6 binds to the *Mesp2* enhancer and promotes gene expression. (*A*) Wild-type and mutant sequences of site B and site D. The bases highlighted in lowercase denote the mutation sites. (*B*) Tbx6 binds to site B and site D. Digoxigenin-labeled oligonucleotide probes containing site B or site D were subjected to EMSA with (+) and without (−) Tbx6. Mutation of the CACAC motif in site B (lane mB1) resulted in the loss of both the wild-type band shifts, whereas mutations in GGGTC (lane mB2) abolished only the upper band. Mutations in the CACAC motif from site D also eliminated the band shift (lane mD). (*C*) β-Gal reporter expression analysis in transgenic mouse embryos with constructs containing either wild-type or mutated *Mesp2* upstream regions. Each of the images is a lateral view with the anterior region toward the top. The numbers of β-gal-positive transgenic embryos are shown in each image (β-gal-positive/transgene-positive).

with a lower mobility and a weaker band with a higher mobility. These two species presumably represent the binding of two and one Tbx6 molecule(s), respectively, because palindromic repeats or spaced tandem repeats of two half fragments of site B generated band shift patterns identical to those of site B (Fig. 6*B*). Tbx6 binding to site B and site D was successfully competed for by oligonucleotides containing the T binding consensus sequence and could be supershifted by incubation of the forming complexes with an anti-FLAG antibody (Fig. 6*A*). We conclude therefore that Tbx6 binds to the upstream region of the *Mesp2* gene by means of the DNA binding activity of its T-box domain.

We next introduced nucleotide substitutions to the conserved CACAC motifs in sites B and D and examined the binding ability of Tbx6 to these mutated oligonucleotide probes. Interestingly, a mutation in site B, designated mB1 (Fig. 2*A*), eliminated both of the wild-type site B band shifts in an EMSA (Fig. 2*B*). Because T-box transcription factors can recognize palindromic sequences and bind to these sites as dimers (13, 14), we introduced nucleotide substitutions to the GGGTC sequence in site B, which is situated in the 5′ region adjacent to the CACAC motif (Fig. 2*A*, mB2). In subsequent EMSA analysis, the mB2 substitution was found to have eliminated only the upper site B band shift, indicating that this mutant oligonucleotide can bind only one Tbx6 molecule (Fig. 2*B*). These results suggest that site B is a partial palindrome that associates with two Tbx6 molecules and that the initial binding depends on the CACAC motif. The site D probe generated one EMSA band, and mutation of the CACAC motif in this site (mD) eliminated this band shift (Fig. 2*B*).

T-box proteins constitute a large family of transcription factors (15). *Tbx18* (16) and *Brachyury* (*Bra*) (17) are expressed in segmented somites and in the tailbud, respectively. Mga is a ubiquitous transcriptional repressor that possesses both T-box and basic helix–loop–helix motifs (18), and the T-box motifs of Mga and Tbx6 show similarities (19). In our present experiments, we examined the DNA-binding abilities of Tbx6, Bra, Mga, and Tbx18 to upstream *Mesp2* sequences using EMSA experiments (Fig. 6*D*). Bra and Tbx18 showed no binding activity to either site B or site D, whereas Mga bound weakly to site B. Taken together, we conclude from these data that Tbx6 is the most likely factor, among the T-box-containing proteins expressed in the PSM, that binds to site B and site D of the *Mesp2* gene.

To examine the function of these upstream *Mesp2* cis elements on gene expression, we performed transient transgenic mouse analyses using a lacZ reporter with mutated cis elements in 6-kb upstream sequences of the *Mesp2* ORF. The nucleotide substitutions that eliminate the binding of Tbx6 to sites B and D of the *Mesp2* promoter (P2EmB1D) diminished gene reporter activity in these assays (Fig. 2*C*). Furthermore, targeted disruption of sites B and D eliminated *Mesp2* expression in the forming somites of homozygous embryos (data not shown), demonstrating that these cis-regulatory elements are essential for somite-specific *Mesp2* expression.

In mouse embryo, *Mesp2* mRNA emerges in anterior PSM, at the position of S-1 (8, 9). Tbx6 protein exists also in S-1 (20). *Mesp2* is not expressed in the PSM of *Tbx6*-null mouse embryos (7), suggesting that it is a downstream target of Tbx6. Although the distinct *Mesp2* signal overlaps only in the anteriormost part of *Tbx6*, the initial *Mesp2* mRNA emerges in the more posterior region, overlapping with the *Tbx6* signal (Fig. 6*E*). These results suggest that Tbx6 is necessary at least for initiation of *Mesp2* expression.

In zebrafish, *fused somite* (*fss*), which encodes *Tbx24*, is known as a distant homolog of mouse *Tbx6*, and the corresponding mutant embryos have neither segmented somite nor *mespb* expression (21). The cis-regulatory elements are also well conserved between the upstream regions of *Mesp2* and *mespb* (Fig. 1*A*), and Tbx24 also binds to the *Mesp2* upstream region (data not shown). Recently, Davidson *et al.* (22) reported that, during heart development in the simple chordate *Ciona intestinalis*, a *Mesp* homolog is also expressed in a Tbx6-dependent manner. Comparing genomic sequences among *Ciona*, mouse, and zebrafish, the authors identified multiple Tbx6 binding sites in the upstream sequence of *Ciona Mesp* homolog. Taken together, we speculate from these findings that Tbx6-mediated activation of the *Mesp* genes is an evolutionally conserved mechanism in Chordata.

The Notch Intracellular Domain (NICD) Activates a *Mesp2* Reporter Construct in a Tbx6-Dependent Manner. To analyze the detailed regulatory mechanisms underlying the control of *Mesp2* expression, we constructed a *Mesp2* reporter system comprising a firefly luciferase reporter and *Mesp2* cis elements. Cotransfection of a Tbx6 expression vector with the *Mesp2* reporter increased luciferase activity by 10-fold (Fig. 3), indicating that Tbx6 functions as a transcriptional activator of *Mesp2*. In somite-stage embryos, *Tbx6* is expressed throughout the PSM and also in the tailbud region (20, 23), whereas *Mesp2* expression is restricted to the anterior PSM just before somite formation, and the expression overlaps only in the anterior limit of the *Tbx6* expression domain (Fig. 6*E*). The discrepancy between these expression patterns strongly indicates that other unknown factor(s) participate in the pathways that restrict the *Mesp2* expression domain to the anterior PSM. Because Notch signaling plays crucial roles in many aspects of somitogenesis, and given that *Mesp2* expression is known to depend on Dll1-Notch signaling (10), we examined the involvement of Notch signaling in the Tbx6-mediated transactivation of *Mesp2*.

The typical Notch signaling pathway is composed of ligands known as DSL (Delta, Serrate, and Lag-2), Notch receptors, effectors known as CSL (CBF-1, Suppressor of Hairless, and Lag-1), and a number of other proteins that modulate the functions of each component of the pathway (24). Once the DSL ligands bind to the Notch receptor, the NICD is proteolytically cleaved, translocates into the nucleus, and binds to its CSL effector (RBPJκ in the case of mouse) to activate the transcription of downstream target genes (24). We transiently introduced expression vectors for NICD and RBPJκ-VP16 (dominant-active RBPJκ) (25), in conjunction with Tbx6, into cultured cells bearing the *Mesp2* reporter. As a positive control, we used the

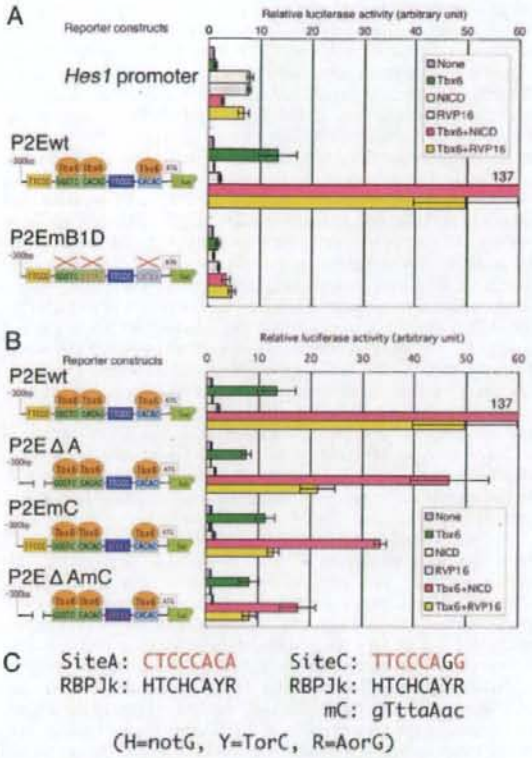

Fig. 3. *Mesp2* expression is activated by Notch signaling in a Tbx6-dependent manner. For each set of analyses, the luciferase activity was normalized to the values obtained in the absence of an expression vector (None). Error bars represent the standard deviation from six independent experiments. RVP16, RBPJκ-VP16. (*A*) Tbx6 activates a *Mesp2*-luciferase reporter gene construct synergistically with the NICD or RBPJκ-VP16. Mutation of site B and site D (denoted as P2EmB1D) eliminates this transactivation. (*B*) Notch signal activates the *Mesp2* reporter construct via site A and site C. The reporter constructs are indicated to the left of the graph. (*C*) Nucleotide sequences of the possible RBPJκ binding sites in site A (*Left*) and site C (*Right*) and the comparison between these regions and the RBPJκ binding consensus sequence (denoted as RBPJk) (27). The nucleotides matching the consensus sequence are shown in red for site A and site C. Nucleotide substitutions in site C (denoted as mC) are indicated in lowercase.

Hes1 promoter, which is known to be a downstream target of Notch signaling (26). Transfection of the *Hes1* reporter construct produced significant luciferase activity even in the absence of NICD (data not shown), reflecting the endogenous NICD activity, and the reporter activity increased further in the presence of either NICD or RBPJκ-VP16. In contrast, neither NICD nor RBPJκ-VP16 was found to activate the *Mesp2* reporter (Fig. 3*A*). However, when NICD and Tbx6 were cotransfected, significant increases in luciferase activity were detected (Fig. 3*A*). RBPJκ-VP16 also can activate the *Mesp2* promoter when cotransfected with *Tbx6* (Fig. 3*A*), suggesting that RBPJκ-dependent Notch signaling activated *Mesp2* reporter in a Tbx6-dependent manner. Consistent with this finding, mutations in site B and site D, which eliminate Tbx6 binding to the *Mesp2* upstream region, greatly reduced *Mesp2* reporter activation by NICD or RBPJκ-VP16 (Fig. 3*A*).

To identify the Notch signaling responsive site within the

Mesp2 upstream region, we analyzed the activity of two additional reporter constructs bearing either a deletion or a mutation in the conserved sites A and C, because these regions contain sequences that have some similarity to the RBPJκ consensus binding site (24, 27) (Fig. 3*C*). We speculated that these sites may play an important role in the regulation of *Mesp2* expression based on our observation that site A is essential for somite-specific expression in combination with site B (Fig. 1). Moreover, reporter activity in forming somites is lost when sequential deletion of the upstream region of the *Mesp2* gene removes a part of site C (11). In our current experiments, the deletion of site A reduced the levels of synergistic activation of the *Mesp2* reporter by both Notch signaling and Tbx6 by up to 50% (Fig. 3*B*, P2EΔA). Reporter activation was also remarkably diminished when we introduced mutations into both site A and site C (Fig. 3*B*, P2EΔAmC), suggesting that the binding of RBPJκ is required for the Tbx6-dependent transduction of Notch signaling. In contrast to the *Hes* family genes, no direct interaction between the Notch signaling pathway and the *Mesp2* regulatory region had been previously identified. Our current findings thus provide the first evidence that *Mesp2* is a direct target of Notch signaling. Furthermore, we identified a regulatory mechanism underlying the Notch signaling pathway that is based on the binding of Tbx6 to transcriptional regulatory sequences (summarized in Fig. 4 *A* and *B*).

We next conducted transient transgenic assays using our lacZ reporters with mutations in sites A and C. Surprisingly, the coexistence of the site A deletion and site C mutation (P2EΔAmC) in our reporter system showed somite-specific β-gal expression, although the activity was slightly weaker than normal (Fig. 5*A*). One possibility that might explain this disparity is that there may be a redundant, RBPJκ-independent pathway of Notch signaling that activates *Mesp2* expression. Consistent with this hypothesis, the P2EΔAmC reporter retained the ability to respond to the coexpression of NICD and Tbx6, although this activity was only 13% of wild-type levels (Fig. 3*B*). Notably, the P2EΔAmC reporter showed no synergistic activation after the coexpression of Tbx6 and RBPJκ-VP16 (Fig. 3*B*), indicating that the ability to respond to RBPJκ-dependent Notch signaling is eliminated by the disruption of sites A and C. These results suggest that Notch signaling activates *Mesp2* expression in both RBPJκ-dependent and RBPJκ-independent manners (Fig. 4*C*). Although most of the Notch signals are mediated by CSL effectors, such as RBPJκ, there is some reported evidence that suggests the existence of RBPJκ-independent Notch signal transduction pathways (28, 29). The molecular components involved in RBPJκ-independent Notch signaling are still poorly understood, but our present data suggest the possibility that Tbx6 not only facilitates RBPJκ-dependent Notch signaling but also acts as a component of an RBPJκ-independent Notch signaling pathway.

Another possible mechanism of somite-specific reporter expression that we observed in our P2EΔAmC transgenic embryos is the involvement of Notch-independent signals (Fig. 4*C*). Although it is clear that Notch signaling is genetically upstream of *Mesp2* activation (9, 10), *Psen1* knockout mouse embryos, which are deficient in Notch proteolysis and therefore do not produce NICD (30), show only moderate decreases in *Mesp2* expression levels (10). Together with our present findings, these observations may indicate that the controlling mechanism for *Mesp2* gene expression is a redundant and robust system and is composed of a number of signaling cascades. Regardless of this possibility, Tbx6 is likely to be essential for all of the signaling pathways involved in *Mesp2* expression, because mutation of the Tbx6 binding sites in the upstream regions of the *Mesp2* gene completely eliminates reporter expression in forming somites (Fig. 2*C*).

Because Tbx6 mRNA (Fig. 6*E*) and protein (20) are distributed throughout the tailbud and posterior PSM, the factors that restrict the expression domain of *Mesp2* in anterior PSM remain to be identified. Notably, although Tbx6 seems to activate reporter expression in cultured cells by itself, dominant-negative RBPJκ(R218H), which retains NICD binding activity but has lost any DNA binding ability (31), inhibits the Tbx6-dependent reporter activation by 50% (Fig. 5*B*). This finding suggests that

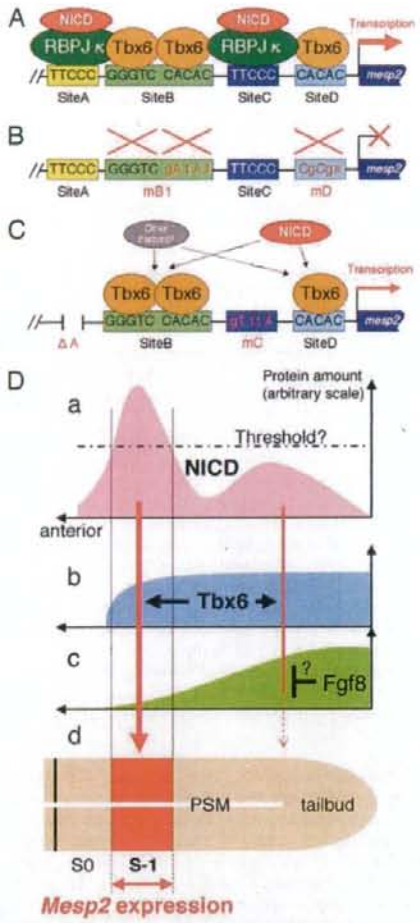

Fig. 4. Proposed mechanisms underlying the control of *Mesp2* expression. Tbx6 and NICD (colored ovals) interact with the conserved upstream sites in the *Mesp2* gene, sites A–D (represented by boxes). Tbx6 binds to site B (two molecules) and site D (single molecule). Site A and site C interact with RBPJκ to achieve a significant increase in *Mesp2* expression levels in the presence of Notch signals (*A*). This activation fully depends on the binding of Tbx6 to site B or site D (*B*). Tbx6 may activate *Mesp2* expression without site A and site C, presumably through an RBPJκ-independent Notch signaling pathway and via other signals (*C*). (*D*) Schematic representation of a proposed model that may explain developmentally regulated *Mesp2* expression in the anterior PSM. (*a*) NICD is highly accumulated in the anterior PSM and less in the posterior (1, 2) to activate *Mesp2* expression (red arrows). There may be a threshold level of NICD accumulation to initiate *Mesp2* activation (broken line). (*b*) Tbx6 protein is distributed in the tailbud and PSM (20) and facilitates *Mesp2* activation by NICD. (*c*) It is possible that the activation of *Mesp2* expression in the tailbud and posterior PSM, if any, is repressed by other factor(s), such as Fgf8 (36), via an unknown mechanism. (*d*) As a result, *Mesp2* expression is restricted in the anterior PSM (red box).

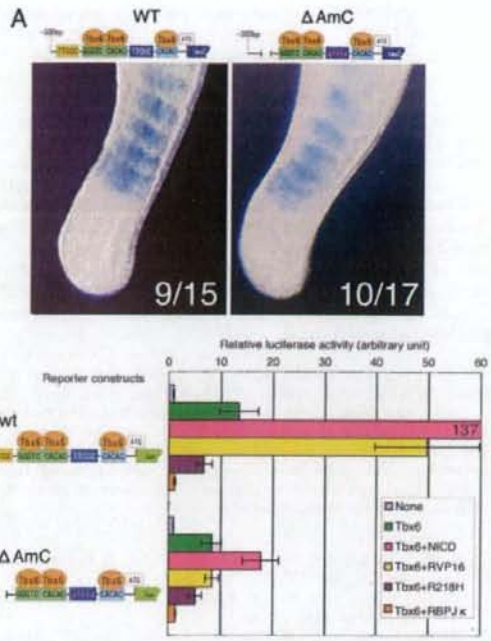

Fig. 5. The expression of *Mesp2* is not achieved solely by RBPJκ-dependent Notch signaling. (*A*) Transgenic analyses reveal that somite-specific reporter expression can still be observed by using the P2EΔAmC construct, which contains a deletion of site A and mutations in site C. The numbers of β-gal-positive embryos are indicated for each image (β-gal-positive/transgene-positive). (*B*) The expression of a dominant-negative RBPJκ diminishes reporter activation by Tbx6 for both the wild-type (wt) and P2EΔAmC (Tbx6+R218H, purple bars) vectors. Wild-type RBPJκ also strongly suppressed reporter activity driven by Tbx6 (Tbx6+RBPJκ, orange bars). Error bars represent the standard deviation in six independent experiments.

Tbx6 itself has only weak transactivation properties, if any, and needs to cooperate with other signals such as Notch for full activity. We speculate that reporter activation by Tbx6 itself (Figs. 3 and 5) may be accomplished by cooperation with Notch signaling, presumably driven by endogenous NICD in cultured cells. Endogenous NICD concentration in cells or tissues is very low and biochemically undetectable (32). However, cultured fibroblast cells express mature Notch protein (33) and show γ-secretase-like activity that generates NICD from Notch protein (32). Furthermore, NICD activates *Hes1* reporter at very low concentrations, below the level of biochemical detection (32). Consistent with these data, *Hes1* reporter showed higher basal activity than *Mesp2* reporters or control reporter with no promoter/enhancer: 100 times higher in COS-7 cells and 60 times higher in NIH/3T3 cells in our observation (data not shown). We suppose that endogenous NICD affects the expression of Notch downstream genes in cultured cells.

NICD accumulation is observed as a strong band-like pattern in the anterior PSM and as a weak diffused signal in the posterior PSM (1, 2). Mesp2 is initially detectable in the middle of a distinct band of NICD in the anterior PSM (2), consistent with the importance of Notch signaling in *Mesp2* expression indicated by our present study. However, the weak Notch signaling activity observed in the posterior PSM may activate *Mesp2* expression, whereas *Mesp2* transcripts appear only in the anterior PSM. One possibility is that there is a "threshold" of NICD levels that is required to trigger Tbx6-dependent *Mesp2* activation (Fig. 4*D*). Because RBPJκ is expressed ubiquitously in the developing embryo (34) and strongly represses Tbx6-dependent activation of the *Mesp2* reporters (Fig. 5*B*), it may also function as a suppressor in the posterior PSM that prevents inadequate expression of *Mesp2*.

Recent reports also indicate that there are two gradients of mutually inhibitory signals, Fgf8 and RA, that have important roles in the positional determination of segment formation (35). It is likely therefore that the Fgf8 and RA signals also participate in the regulation of *Mesp2* expression. Recently, Delfini *et al.* (36) reported an intriguing result suggesting that Fgf signaling represses *Mesp* expression. Using *in ovo* electroporation, they demonstrated that the up-regulation of Fgf in the PSM diminishes the endogenous expression of *cMeso*, the chick *Mesp* homolog. It is plausible therefore that Fgf8, which is strongly expressed in the tailbud and posterior PSM, prevents the inadequate expression of *Mesp2* in posterior region. The involvement of RA in *Mesp2* expression remains elusive, however, because the disruption of *CYP26* (37), a degradation enzyme for RA, does not severely affect *Mesp2* expression levels (2). In the zebrafish embryo, FGF signaling up-regulates a basic helix–loop–helix transcription factor, her13.2, which maintains the oscillation of the Notch signals in both the tailbud and PSM by repressing the Notch-regulated genes *her1* and *her7* (38). RA and Fgf signals may thus contribute to the positioning of *Mesp2* expression by coordinating the regular oscillation of Notch signals in the tailbud and PSM.

Interestingly, it has been revealed that *Tbx6* is one of the direct targets of RBPJκ-dependent Notch signaling (39). During somitogenesis, Notch signals may first activate *Tbx6* expression in the tailbud and posterior PSM region and then activate *Mesp2* expression in the anterior PSM in cooperation with Tbx6. Furthermore, Tbx6 also works upstream of the Notch signaling pathway. In embryos of *Tbx6* hypomorphic mutant mice, *Dll1* expression in the tailbud and posterior PSM is greatly reduced (40). Promoter analyses of *Dll1* have demonstrated that Tbx6, in synergy with Wnt signaling, activates *Dll1* expression by binding to T-binding consensus sequences (20, 41). Taken together, our present results demonstrate that Tbx6 and Notch signaling constitute a regulatory network that controls somite formation via the regulation of *Mesp2* expression.

Materials and Methods

Transgenic Analyses. DNA fragments, with and without mutations in conserved upstream sites, were generated from a *Mesp2* genomic fragment by using a standard PCR-based protocol. Transgene inserts were digested from the corresponding plasmids, purified, and injected into the male pronucleus of a fertilized egg (42). The injected embryos were then transferred into pseudopregnant recipients and allowed to develop until 9.5–10.5 days postcoitum. Embryos were then analyzed for lacZ expression by X-gal staining (43) and subsequently examined for the presence of the transgene by PCR analysis (44).

Yeast One-Hybrid Screening. Synthetic oligonucleotides corresponding to contiguous sequences of conserved site A (nucleotides −199 to −191 from first ATG of *Mesp2* ORF) and site B (nucleotides −162 to −140) were inserted into the vectors pHISi-1 and placZi (Clontech), immediately upstream of the HIS3 and lacZ reporter genes, respectively. The resulting constructs were then linearized and introduced simultaneously into *Saccharomyces cerevisiae* YM4271 (Clontech) to generate the bait strain. The bait strain was then transformed by using 80 μg of 11.5 days postcoitum mouse tail cDNA library plasmid (45) to screen up to 2 million independent clones. We obtained hundreds of positive clones (HIS3+ and LacZ+) and recovered

DEVELOPMENTAL BIOLOGY